Physiologia Plantarum

ORIGINAL RESEARCH OPEN ACCESS

Characterization of Phytoene Desaturase Knockout Carotenoid-Deficient Microalgal Mutants Generated by Cas9-Ribonucleoprotein Complexes

Ana Molina-Márquez[1] | Simon Kelterborn[2] | Peter Hegemann[3] | Miguel Pérez-Rodríguez[4] | Javier Vigara[1] | Rosa León[1]

[1]Laboratory of Biochemistry, Center for Natural Resources, Health and Environment (RENSMA). University of Huelva, Huelva, Spain | [2]Institute of -Translational Physiology, Charité-University of Berlin. Charité Platz 1, Berlin, Germany | [3]Institute of Biology, Experimental Biophysics, Humboldt-University of Berlin, Berlin, Germany | [4]Department of Cell Biology, Physiology and Immunology, University of Córdoba, Campus of International Agri-Food Excellence CeiA3, Córdoba, Spain

Correspondence: Rosa León (rleon@uhu.es) | Ana Molina-Márquez (ana.molina@dqcm.uhu.es)

Received: 1 December 2023 | **Revised:** 13 January 2026 | **Accepted:** 15 January 2026

Handling Editor: A. Krieger-Liszkay

Keywords: carotenoids | *Chlamydomonas reinhardtii* | CRISPR | PDS | phytoene desaturase | plastoquinone | transcriptomics

ABSTRACT

Phytoene desaturase (PDS; EC 1.3.5.5) is a key enzyme of the carotenoid biosynthetic pathway, catalyzing the desaturation of phytoene, precursor of all carotenoids. In this study, several *PDS*-knockout (*PDS*-KO) transformants of the chlorophyte microalga *Chlamydomonas reinhardtii* were generated using a reverse genetics strategy. Two single guide RNAs (sgRNA) were designed to target the first exon of the *PDS* gene, and pre-assembled Cas9 ribonucleoprotein (RNPs) complexes were delivered into microalgal nuclei by electroporation. Multiple white *PDS*-KO transformants were successfully obtained by this approach, and three independent transformant lines were subsequently characterized. By integrating ultrastructural, pigment and transcriptomic analyses of dark-grown cells of several *PDS*-KO carotenoid-deficient mutants in comparison with the parental strain, it was demonstrated that carotenoids are indispensable components of multiple cellular architectures. Chromatographic analysis confirmed that the only carotenoid accumulated in these transformants was phytoene, which lacks the critical structural and photoprotective functions of its colored derivatives. Transmission Electron Microscopy (TEM) observations revealed profound ultrastructure alterations, including poorly developed chloroplasts and effects on other cellular structures that were either absent or severely disorganized. Consistently, clustering differentially expressed genes into functional groups revealed downregulation of pathways associated with photosynthesis, chlorophyll and carotenoid biosynthesis, ribosome biogenesis, and vesicle and membrane trafficking in the *PDS*-KO lines. Conversely, upregulation of regulatory and retrotransposon-inducing genes was observed. These findings underscore the central metabolic role of colored carotenoids in plant cells, highlighting their essential contribution to cellular homeostasis and photosynthetic competence.

1 | Introduction

Carotenoids constitute a diverse group of lipophilic isoprenoid compounds widely distributed in nature that participate in different metabolic and cellular functions (Britton et al. 2004). In microalgae, as in higher plants, carotenoids are indispensable structural components of the photosystems, where they are involved in light harvesting, energy transfer, and protection of the photosynthetic apparatus against photooxidative damage (Varela et al. 2015). They are also constituents of the eyespot, a

specialized organelle of many flagellated microalgae exhibiting photo movement responses (Hegemann 1997; Ueki et al. 2016). In addition, carotenoids and their derived apocarotenoids are precursors for the synthesis of plant phytohormones and growth regulators (Felemban et al. 2019). Moreover, carotenoids contribute to the stabilization of cell membranes under stress conditions (Mikami and Murata 2003), and play an important role in signal photoreception and photoheterotrophic metabolism in numerous bacterial species, serving as secondary chromophore antennas that transfer solar energy to retinal in a broad spectrum of microbial rhodopsin proteins (Chazan et al. 2023).

Carotenoids cannot be synthetized by animals, including humans. Nevertheless, due to their antioxidant, free radical-scavenging, pro-vitaminic and pigmenting properties, they are considered to play an important role in the health of both humans and animals, which must acquire them through their diet (Rodriguez-Concepcion et al. 2018; Mapelli-Brahm et al. 2023). For this reason, carotenoids are widely demanded as functional ingredients, additives, and supplements in the food and feed sectors (Schüler et al. 2017; Novoveská et al. 2019). Although uncolored carotenoids have received less attention than their colored counterparts, recent studies have revealed their numerous beneficial properties (Mapelli-Brahm and Meléndez-Martínez 2021). Phytoene (7,8,11,12,7′,8′,11′,12′-octahydro-ψ,ψ-carotene) is a uncolored C40-carotenoid with a strong absorption in the UV region that has been reported to exhibit multiple health-promoting properties, including antioxidant, anticancer, anti-inflammatory, skin-whitening and anti-aging effects (Meléndez-Martínez et al. 2019; Morón-Ortiz et al. 2024; Perazzoli et al. 2024). All these benefits have contributed to the increasing demand for phytoene, whose global market is expected to grow at an annual rate of 3.4% until 2029 (Absolute Markets Insights 2023).

From the metabolic point of view, phytoene is produced by condensation of two molecules of geranylgeranyl pyrophosphate (GGPP) in a reaction catalysed by phytoene synthase (PSY). 15-cis-Phytoene is converted into 9,15,9′-tricis-ζ-carotene, via the intermediate 15,9′-dicis-phytofluene, by the phytoene desaturase (PDS, EC:1.3.5.5). 9,15,9′-tricis-ζ-carotene is subsequently converted into the fully desaturated lycopene by the sequential action of 15-cis-zeta-carotene isomerase (Z-ISO), ζ-carotene desaturase (ZDS) and carotene isomerase (*CRTISO*), which catalyses the conversion of pro-lycopene (7,9,7′,9′-tetracis-lycopene) to all-trans lycopene, from which the rest of the cycled carotenoids and xanthophylls are synthetized (Figure 1A).

All these desaturation reactions increase the number of conjugated double-bonds from three in phytoene to eleven in lycopene, thereby causing a progressive shift in the maximum absorption of these compounds from the UV to the visible region of the spectrum. Blocking the carotenoid biosynthetic pathway at the level of *PDS* hold the synthesis of colored carotenoids and lead to phytoene accumulation (Molina-Márquez et al. 2019).

PDS is a plastid-localized, membrane-associated FAD-dependent desaturase enzyme that extracts electrons from phytoene and phytofluene, transferring them to plastoquinone, via FAD as redox cofactor, thereby linking carotenoid desaturation to the electron transport chain (Grossman et al. 2004; Lohr et al. 2005; Gemmecker et al. 2015; Koschmieder et al. 2017). In *C. reinhardtii*, phytoene desaturase is a protein of 564 aa that shares high sequence similarity with other algal and plant PDS proteins, while it has no sequence homology with the corresponding bacterial or fungal phytoene desaturase, CRTI. The enzyme contains a typical chloroplast transit peptide at the N-terminal end and the characteristic dinucleotide FAD-binding domain (Tran et al. 2012) (Figure 1B–D).

The study of mutants of the carotenoid pathway in both microalgae and plants, and more recently the target knockout of specific genes of the pathway by genome editing technologies, has contributed to deciphering this metabolic route (Gupta and Hirschberg 2022). However, many regulatory aspects and the influence of carotenoids in different physiological and cellular processes are still unclear. Most of the enzymes involved in the carotenogenic biosynthetic pathway in *C. reinhardtii* have been identified through analysis of pigment-deficient mutants and by comparing the affected loci with their corresponding orthologous plant genes (Grossman et al. 2004; Lohr et al. 2005). Nevertheless, PDS-deficient mutants remained difficult to obtain for a long time. The first *Chlamydomonas* white mutants obtained by traditional mutagenesis were found to be affected in the phytoene synthase gene (*PSY*) (McCarthy et al. 2004). Similarly, in *Arabidopsis*, the first albino mutants obtained were affected in the synthesis of the PDS cofactor plastoquinone (Norris et al. 1995) or in the plastid terminal oxidase, PTOX (Carol et al. 1999). The first *PDS* mutant, obtained by random mutagenesis in *C. reinhardtii* (*pds-1*), had only a partially affected PDS enzyme and did not accumulate phytoene, despite having a reduced content of colored carotenoids (McCarthy et al. 2004; Tran et al. 2012). Attempts to knock-out the gene encoding phytoene desaturase through small RNA interference and antisense strategies likewise failed to produce phytoene-accumulating transformants (Vila et al. 2008).

The difficulty in obtaining PDS mutants was originally attributed to: (i) the possible existence of more than one phytoene desaturase gene in the genome of *Chlamydomonas*, (ii) the extreme sensitivity to light of carotenoid-less mutants or (iii) the toxicity of phytoene. Finally, Tran et al. (2012) successfully generated two *PDS* knockout-mutants, by UV-induced and insertional mutagenesis, respectively. The complete inability of these mutants, denoted as *pds1*-2 and *pds 1–3*, to synthesize carotenoids beyond phytoene confirmed the existence of a single PDS-encoding gene in *Chlamydomonas*.

The existence of a gene with high homology to the bacterial *CRTI*-type phytoene desaturase (Cre12.g541750) has been recently reported in *Chlamydomonas* (Lohr 2023). This *CRTI*-type gene, which has also been found in other algal genomes and seems to be absent in higher plants, cannot replace PDS activity nor produce lycopene, unlike its bacterial homologs. In *C. reinhardtii*, the biological function of the *CRTI*-like gene remains unknown (Lohr 2023).

In this study, we generated targeted *PDS* knockout transformants using a reverse genetics approach and conducted a comprehensive characterization of the resulting lines, examining their cellular components and, for the first time, investigating the transcriptomic effects of carotenoid absence in *Chlamydomonas*.

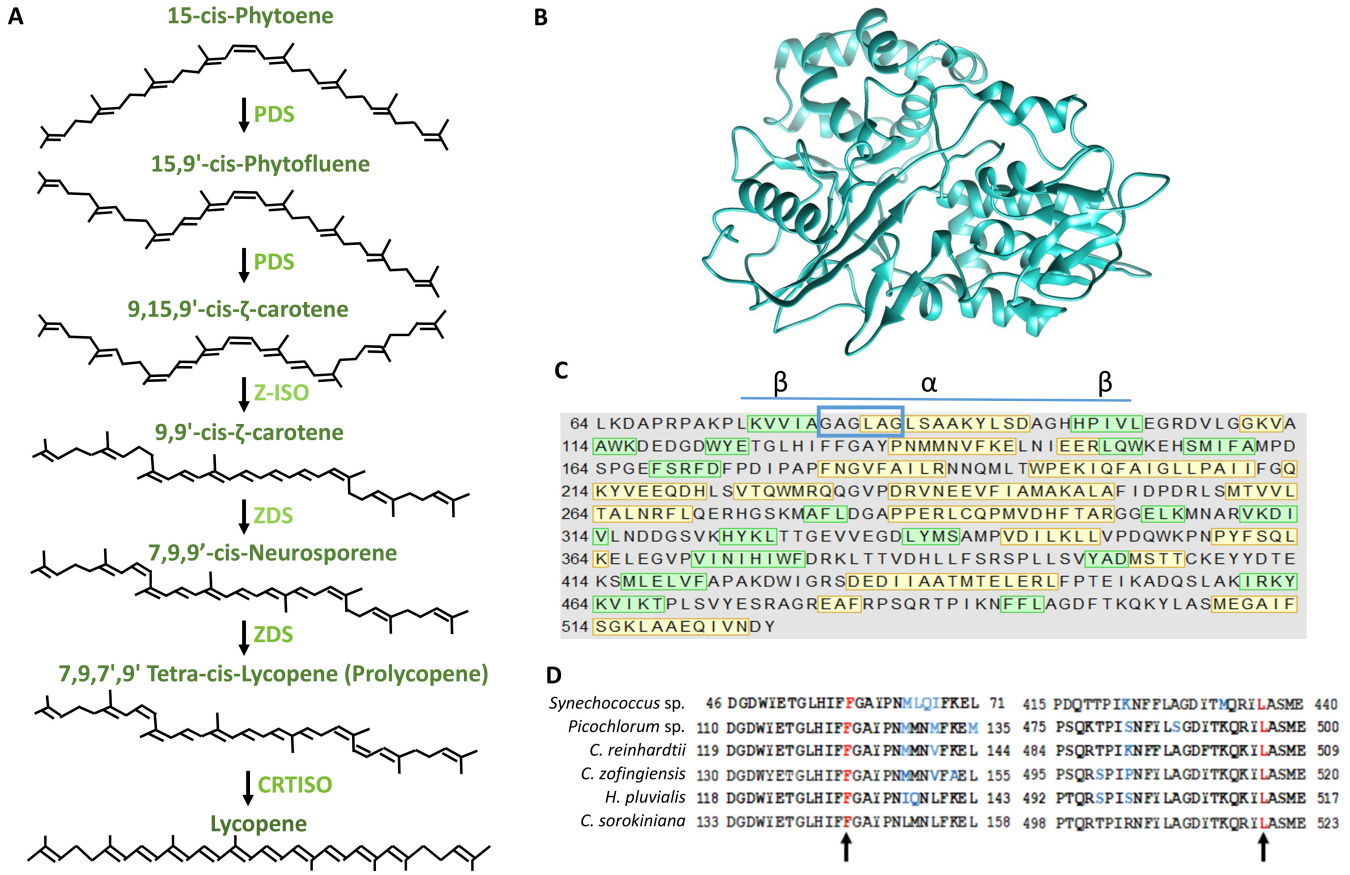

FIGURE 1 | Desaturation steps in the carotenoid biosynthetic pathway in plants, and structural and sequence features of *Chlamydomonas reinhardtii* Phytoene desaturase. (A) Desaturation steps within the carotenoid biosynthetic pathway. (B) Predicted 3D structure of CrPDS generated using the Phyre2 modeling software and visualized with UCSF Chimera version 1.16. (C) 2D structure of CrPDS, α helixes are shaded in yellow and β strands in green; the conserved β-sheet–α-helix–β-sheet segment of the Rossmann fold is indicated with an overline, and the consensus motif (GAGxxG), characteristic of this dinucleotide-binding fold, is highlighted in a blue box. (D) Sequence alignment of selected PDS fragments with indication of key aminoacid residues (↑) required for the action of the herbicide norflurazon. Accession numbers for the compared sequences are MAX88086.1 (*Synechococcus* sp. SAT82); KAI8106466.1 (*Picochlorum* sp.); XP_005850369.1 (*Chlamydomonas reinhardtii*); ABR20877.1 (*Chromochlorosis zofingienses*); AK071906.1 (*Haematococcus pluvialis*); PRW56502.1 (*Chlorella sorokiniana*).

2 | Materials and Methods

2.1 | Strain and Culture Conditions

C. reinhardtii strain CC-3403 (RU-387 *nit1 arg7 cw15 mt2*) was obtained from *Chlamydomonas* Resource Center (http://www.chlamycollection.org) and grown in liquid or agar solidified standard Tris-acetate phosphate (TAP) medium supplemented with 100 μg mL^{-1} of L-arginine (TAP-Arg), under continuous white light of 150 μE m^{-2}s^{-1} or in synchronized cultures (cycles of 14 h at 25°C under light and 10 h at 18°C in the darkness). Transformed microalgae were cultured in darkness without addition of arginine.

2.2 | In Vitro Testing of Cas9-gRNA Ribonucleoprotein Complexes (RNP)

Two Cas9-gRNA Ribonucleoprotein complexes were designed for the targeted cleavage of the *PDS* gene from *C. reinhardtii* (Cre12.g509650) using standard software (Haeussler et al. 2016) and prepared as previously reported (Sizova et al. 2021). A control RNP that targets the SNF1-related protein kinase (*SNRK2.2*) encoding gene (Cre12.g499500) was also included. SNRK2.2 represses S-inducible genes, and its knockout induces the constitutive expression of the easily detectable arylsulfatase (*ARS*) gene, even in S-replete media, as previously described (Kelterborn et al. 2022). Briefly, crRNA and tracrRNA were chemically synthesized by Integrated DNA Technologies and annealed by mixing equimolar amounts of both RNA fragments in DUPLEX buffer (100 mM potassium acetate, 30 mM HEPES, pH 7.5; Integrated dNA Technologies), heating at 95°C for 2 min and cooling down with a rate of 0.1°C min^{-1}, producing the guide RNA (gRNA). The recombinant spCas9 protein was expressed in *E. coli* using pET-28b-Cas9-His for expression (Addgene plasmid, 47,327) and purified by two subsequent steps with Ni-NTA column and gel filtration as previously reported (Kelterborn et al. 2022). The RNP complexes were assembled by mixing equimolar amounts of functional gRNA and the spCas9 protein in 10 X Buffer O (00.5 M Tris–HCl, pH 7.5, 100 mM $MgCl_2$, 1 M NaCl and 1 mg mL^{-1} BSA; Integrated and Technologies) to a final concentration of 3 μM and incubating at 37°C for 15 min. The effectiveness of the RNPs complexes was tested in vitro using PCR-amplified DNA fragments corresponding to the targeted

regions of the *PDS* gene. These fragments were purified, incubated with the respective pre-assembled RNP complexes, and the resulting cleavage products were analyzed by electrophoresis. The characteristics of the primers used for these amplifications are shown in Table S1.

2.3 | Generation of PDS Knockout *Chlamydomonas* Transformants

Synchronized cell cultures were transformed by electroporation according to a previously optimized protocol (Sizova et al. 2021). The cultures were kept in the exponential growth phase for at least 10 days by periodical dilutions with fresh TAP-Arg medium every 3–4 days. When the cellular density was 1–3 $\times 10^6$ cells mL^{-1} and the culture was at the end of the light phase, cells were harvested by centrifugation (2000 × g, 10 min at room temperature) and resuspended in MAX Efficiency transformation medium (A24229; Thermo Fisher Scientific) supplemented with 40 mM sucrose, to get a concentrated cell suspension of 10^8 cells mL^{-1}. The concentrated cell suspension was heat-shocked at 40°C for 30 min and 350 rpm (Thermomixer) and electroporated according to the manufacturer's instructions in a NEPA21 electroporator (Nepa Gene Co.). For each transformation reaction, 40 μL of concentrated cell suspension were mixed with 3 μL of 3 μM RNP and 0.5 μg of the plasmid (pARG7 230), which contains the selectable argininosuccinate lyase (*ARG7*) gene, that complements the defective corresponding gene in the *Chlamydomonas* arginine-auxotrophic strain (Kelterborn et al. 2022) and double-stranded donor DNA sequence (dsDR) with stop codons in the 6 open reading frames, incorporated to improve the transformation efficiency and, in addition, ensure the knockout of the *PDS* gene by the insertion of a stop codon into the cleavage site (Greiner et al. 2017).

The conditions used for the electroporation were two 8 ms/200 V poring pulses at 50 ms intervals with a decay rate of 40% and followed by five 50 ms/20 V polarity-exchanged transfer pulses at 50 ms intervals with a decay rate of 40%. The impedance ranged between 400 and 550 Ω. After electroporation, fresh TAP-Arg liquid medium was added to the cells that were placed under darkness overnight. After this incubation, cells were spread onto solid TAP selective medium. The dsDR were obtained by mixing equimolar concentrations of the corresponding sense and antisense oligonucleotides with three phosphorothioate-protected bonds at each end. The annealing was performed in duplex buffer (100 mM potassium acetate and 30 mM HEPES, pH 7.5) at 95°C for 2 min, followed by a slow cooling step (at a rate of 0.1°C/min).

2.4 | Screening of PDS Algal Mutants

The screening of the obtained transformants was performed by PCR using Phire Plant Direct PCR Master Mix (Thermo Fisher Scientific), specific primers designed to detect the expected mutation, and the cell lysates as template. The crude cell extracts were prepared by transferring 80 μL of each cell culture into a 96-well V-bottom plate, which was subsequently centrifuged at 2500 × g for 10 min, at room temperature. After removing the supernatant, the cells were resuspended in 20 μL of lysis dilution buffer, incubated at room temperature for 5 min and centrifuged at 2500 × g for 10 min. This lysate supernatant was used as DNA template in PCR with specific primers designed to detect the regions targeted by RNP complexes in the *PDS* gene (Table S1). The PCR conditions were: an initial denaturation at 98°C for 5 min, 37 cycles of a denaturation at 98°C for 12 s, annealing at 70°C for 12 s and elongation at 72°C for 60 s, followed by a final elongation at 72°C for 4 min. The PCR products with unexpected size were sequenced to confirm the knockout mutations.

2.5 | Determination of Carotenoids

Carotenoids were extracted with methanol as previously described (Lichtenthaler 1987). Chromatographic analysis of the carotenoid extracts was performed in a Merck Hitachi HPLC system equipped with a diode-array detector, according to the method described by Young et al. (1997). Separation was achieved on an RP-18 Nucleosil C18 column (100, 5 μm particle size, 250 × 4.6 mm; Analisis Vínicos). The flow rate was 1 mL min^{-1}, and 100 μL of sample was injected for each run. The mobile phases used were: Solvent A (ethyl acetate 100%) and solvent B (acetonitrile:H_2O; 9:1 v/v). The gradients applied were: 0–16 min 0%–60% A; 16–30 min 60% A; and 30–35 min 100% A. Standards for lutein, zeaxanthin, β-carotene, neoxanthin, violaxanthin were obtained from MERCK-SIGMA or DHI. The phytoene standard was kindly provided by Dr. Melendez (University of Seville, Spain). All measurements were performed in triplicate, and results are expressed as mean values ± standard deviation.

2.6 | Dry Weight Determination

Dry weight was determined by filtering an exact volume of microalgae culture (5 mL) on pre-tared glass-fiber filters (GF/F Whatman). Filters were dried at 80°C for 24 h and weighed on an analytical balance to calculate the dry weight by difference. Values are the average of three measurements.

2.7 | Isolation of Knockout Cell Lines by Fluorescence-Activated Cell Sorting (FACS)

PDS knockout transformant lines were obtained by co-transformation with plasmid pARG7, which complements arginine auxotrophy, and selected on arginine-deficient medium. To ensure the absence of transformants that have acquired the plasmid without undergoing knockout, as well as to exclude interference from possible revertants, liquid cultures of transformants were subjected to fluorescence-activated cell sorting (FACS). Samples were filtered through a 50 μm nylon mesh and analyzed in a BD FACSJazz Cell Sorter, equipped with two lasers of 488 and 561 nm and seven detectors. Side Scatter signal was plotted against Forward Scatter (FSC) signal to select the desired population and eliminate possible bacterial contaminant population of smaller size. Doublets were discarded by plotting FSC-area against FSC-height. White, chlorophyll-deficient cells were sorted on the basis of the chlorophyll

fluorescence signal detected through a red (670/40 nm) band-pass filter following excitation with a blue laser.

2.8 | Microscopy

Optical microscopy images were obtained using an Motic BA410E microscope. For Transmission electronic microscopy (TEM), samples were collected by centrifugation and fixed with 1.6% glutaraldehyde in cacodylate buffer 0,1 M, pH 7.2 (CB), at 4°C during 1 h. The samples were washed three times with CB and post-fixed with CB containing 1% osmium tetroxide for 1 h at 4°C. Subsequently, samples were dehydrated in an acetone series (50%–100% v/v acetone in water) and embedded in Spurr resin. Sections were stained with 2% uranyl acetate and lead citrate. Finally, sections were examined with a Libra 120 Pils Carl Zeiss TEM microscope and photographed.

2.9 | RNA Extraction

Cultures of *C. reinhardtii* parental line cells (grown on TAP-Arg medium in darkness for 96 h) and *PDS* knockout transformant cells grown in darkness without arginine, as described in Section 2.1. of Material and Methods, were sorted by FACS as indicated above to ensure separation from non-*PDS* Knockout transformants. Six independent samples from the parental line and six samples from the selected transformants (four from ΔE10, one from ΔA2 and one from ΔD2) containing about 10^6 cells were spun down by centrifugation and resuspended in 100 μL of Trizol LS (Invitrogen). The lysate was pipetted up and down several times to homogenize it and frozen at −80°C. Total RNA was extracted using the standard TRIzol protocol, following the manufacturer's instructions and used for library preparation and sequencing. Integrity of the extracted RNA was checked by an Agilent-2100 bioanalyzer. RNA concentrations and RIN values higher than 963 pg/μL and 7, respectively, were obtained for all the samples.

2.10 | Library Preparation, Sequencing, and Generation of Count Tables

For the library preparation, mRNA was processed as previously described, following an adapted version of the single-cell mRNA seq protocol of CEL-Seq (Hashimshony et al. 2012; Simmini et al. 2014). In brief, samples were barcoded with CEL-seq primers during reverse-transcription and pooled after second-strand synthesis. The resulting cDNA was amplified by an overnight in vitro transcription reaction. Sequencing libraries were prepared with Illumina Truseq small RNA primers. The DNA library was paired-end sequenced on an Illumina Nextseq 500, high output, with a 1 × 75 bp Illumina kit (R1: 26 cycles, index read: 6 cycles, R2: 60 cycles). The first read was used to identify the Illumina library index and CEL-Seq sample barcode. The second read was aligned to the *C. reinhardtii* 281_v5.6 reference transcriptome using BWA MEM (Li and Durbin 2010). Reads that mapped to multiple locations were discarded. Mapping and counting of reads were performed using the MapAndGo script (https://github.com/anna-alemany/transcriptomics/tree/master/mapandgo).

2.11 | Differential Expression and Functional Enrichment Analysis

Differential expression analysis was performed with the DEA-Transcriptomic module of the OmicsBox software (Biobam Bioinformatic solutions), using the weighted trimmed mean of M-values (TMM) method to normalise library sizes and the EdgeR quasi-likelihood F-test of EdgeR package with robust settings for statistics (Robinson et al. 2009). Genes that exhibit a $\log_2$ fold change greater than 1 and lower than −1, at a false discovery rate (FDR) < 0.05, were defined as significantly different between control and knockout strains. Functional enrichment for the differentially expressed gene collections was carried out with ALGAEFUN software (Romero-Losada et al. 2022).

2.12 | Quantitative Real-Time PCR (qRT-PCR) Analysis

Quantitative PCR (qPCR) assays were conducted in triplicate using the Mx3000P Multiplex Quantitative PCR System (Stratagene) with 1 μL of cDNA as template and Brilliant SYBR Green QPCR Master Mix (Stratagene, Agilent Technologies). The thermal cycling protocol consisted of an initial activation step at 95°C for 10 min to activate the Hot Start Taq polymerase, followed by 40 amplification cycles comprising denaturation at 95°C for 30 s, annealing at 60°C for 30 s, and extension at 72°C for 30 s. Each reaction was performed in triplicate using gene-specific primers (Table S2). As the expression of the *CBLP* gene, which encodes a component of 40S small ribosomal subunit (GenBank accession X53574), has been demonstrated to remain stable under varying light conditions (Im and Grossman 2002), *CBLP* was employed as housekeeping gene to normalize mRNA abundance. Relative gene expression levels were calculated using the $2^{-\Delta\Delta CT}$ method (Pfaffl 2001).

3 | Results and Discussion

3.1 | Generation of Efficient PDS-Targeting RNP Complexes

Two single guide RNAs (sgRNAs) were designed for the targeted mutagenesis of the *PDS* gene in the green microalga *C. reinhardtii*. In this model chlorophyte, phytoene desaturase is encoded by a nuclear gene of 4080 bp, located in chromosome 12 of the nuclear genome (Cre12.g509650) with 6 exons and 5 introns (Tran et al. 2012). The first 186 nucleotides encode for a typical chloroplast transit peptide of 62 aa, located at the N terminus of the protein. The Cas9 ribonucleoprotein (RNP) complexes, RNP1 and RNP2, were generated to specifically target the first exon region, between the nucleotides 132–151 and 147–166 of the *PDS* gene, respectively (Figure 2A).

Detailed sequences of the sgRNA spacers, as well as the target regions within the *PSD* gene of *C. reinhardtii* are shown in Figure 2B. The designed gRNAs were assembled with the endonuclease Cas9 protein from *Streptococcus pyogenes* (spCas9), and the cleavage activity of the preassembled complexes, RNP1 and RNP2, was tested in vitro as described in M&M. It was confirmed that Cas9 protein is accurately guided by both RNP complexes to the target *PDS* fragments, where it introduces a

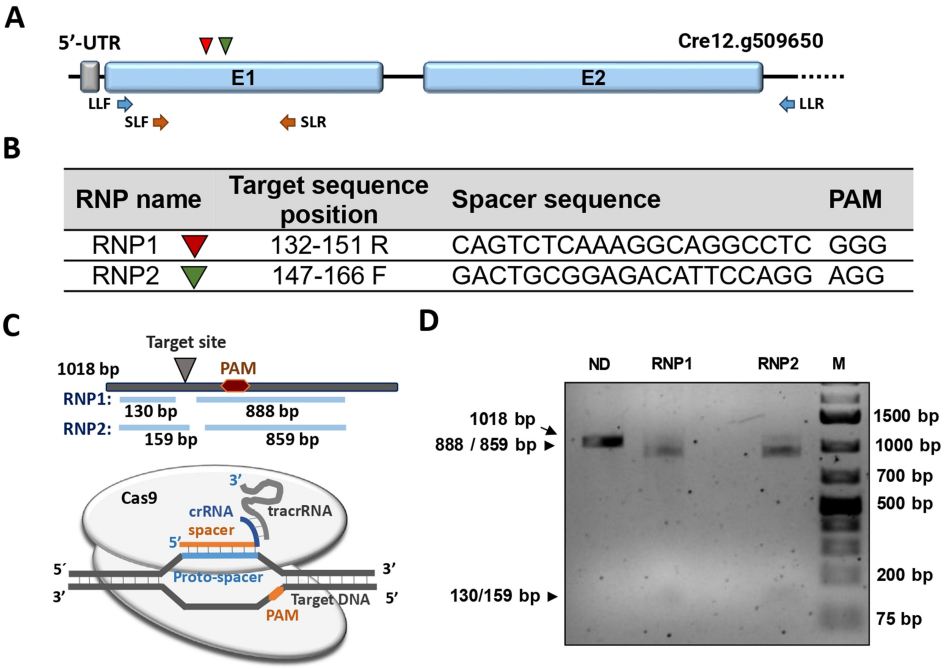

FIGURE 2 | **Preparation of functional Cas9-gRNA Ribonucleoprotein complexes (RNP).** (A) Structure of the *PDS* gene with indication of the targeting sites for RNP1 (▼) and RNP2 (▼) ribonucleoprotein complexes; blue boxes represent exons; black lines represent introns; blue and red arrows indicate the annealing sites of the designed primers to detect the expected mutation (Table S1). (B) Sequence of the two spacer sequences used. (C) Schematic design of the assembled Cas9-NRP complexes interacting with the target DNA, and (D) electrophoretic analysis of the in vitro effectiveness of RNP1 and RNP2 complexes on a 1018-nucleotide PCR-amplified fragment of the *PDS* gene. SL and LL denote the positions of the PCR primer pairs used in this study. ND states for nondigested DNA template.

double-strand break, generating DNA fragments of the expected size (Figure 2C,D).

3.2 | In Vivo Disruption of *Chlamydomonas PDS* Gene by Cas9/sgRNA Ribonucleoprotein Complexes

The two preassembled Cas9 single-guide RNA (Cas9/sgRNA) ribonucleoprotein complexes, RNP1 and RNP2, were subsequently employed for the targeted knockout of the *PDS* gene in *C. reinhardtii* cells. Both RNP complexes were delivered into the microalgal nucleus by electroporation, together with a plasmid carrying the *ARG7* selectable gene (pARG7 230), which complements the argininosuccinate lyase gene in the arginine-auxotrophic host species. The initial difficulties reported by several authors regarding the efficient expression of Cas9 in *Chlamydomonas* have been overcome by the successful delivery of RNP complexes, which have demonstrated high efficiency in knocking out multiple genes of this microalga. The RNP approach has important advantages over nuclear *Cas9* expression: such as a faster and more efficient effect, due to the fact that the *Cas9* gene does not need to be integrated in the algal genome and the synthesized protein does not have to be accurately refolded in the *Chlamydomonas* cell. In addition, off-target effects of CRISPR are minimized, since the Cas9 enzyme and the corresponding gRNA are not accumulating in the cell for a prolonged time (Baek et al. 2016; Greiner et al. 2017).

The co-transformation with RNP complexes and pARG7 230 plasmid yielded around 30 colonies of *C. reinhardtii* per μg DNA for RNP1; 45 colonies per μg DNA for RNP2 and 190 colonies per μg DNA for the control RNP, targeted to the *SNRK2.2* gene. Between 30% and 50% of the transformants obtained with RNP1 or RNP2 appeared as white colonies. The white phenotype indicates the lack of colored carotenoids and the probable knockout of the *PDS* gene. Fifty white mutant lines were analyzed at the molecular level. Fragments of the *PDS* spanning 1018 nucleotides in the parental line, containing the target sequence, were amplified by PCR for each mutant line, and the length of the resulting amplicons was compared with that of the parental line by electrophoretic analysis, as shown in Figure 3A. In some cases, no amplification was observed, possibly due to the insertion of very big DNA fragments or to the occurrence of big deletions. Some transformants showed amplicons longer than the control, indicating the insertion of DNA fragments of moderate length. Nine of these transformants were further analysed by sequencing the obtained amplicon. Alignment of the RNPs-targeted sequences from the wild type (WT) and selected *PDS*-mutant lines revealed that most mutations consisted of insertions of the pARG7 230 plasmid fragments, ranging in size from 47 to at least 2078 nucleotides. Some of the mutant lines analysed had additionally incorporated sequences of unknown origin and/or exhibited deletions ranging from 2 to at least 42 nucleotides (Figure 3B).

Three of the *PDS*-edited mutants that exhibited the greatest growth ability, Δ3403-E10 (ΔE10), Δ3403-A2 (ΔA2), and Δ3403-D2 (ΔD2) were selected for further characterization. At the molecular level, the mutant ΔE10 possesses a truncated *PDS* gene due to an insertion–deletion at position 159 within the first exon. The mutation occurred three nucleotides upstream of the protospacer-adjacent motif (PAM) sequence.

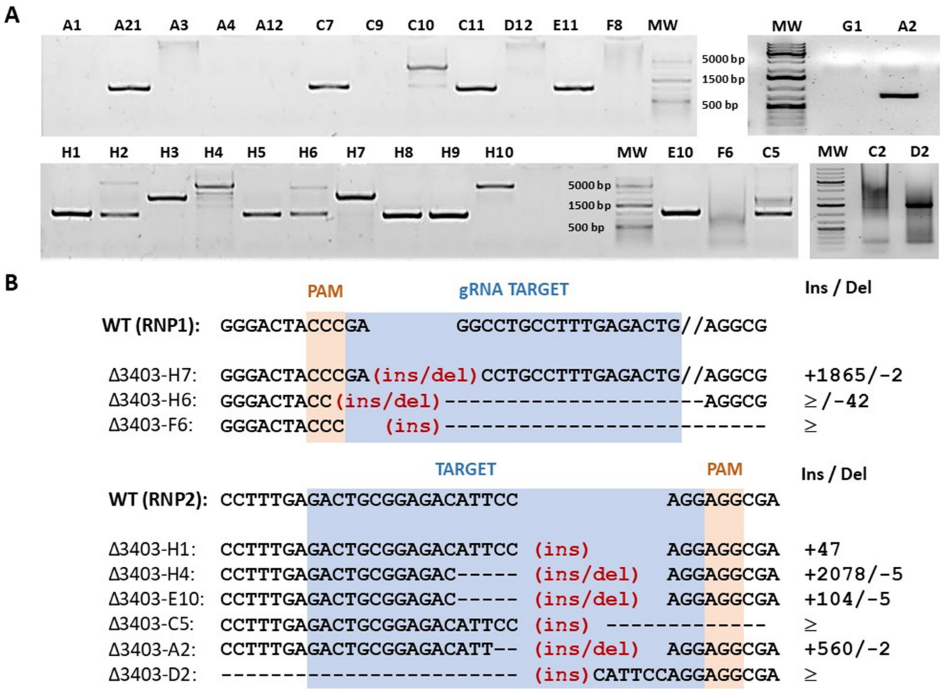

FIGURE 3 | Molecular analysis of transformant colonies. Amplification of *PDS* fragments of 1018 nucleotides, using specific primers (Table S1) designed to detect the targeted regions (A). Alignment of the target sequence in the *PDS* gene of wild-type (WT) and nine *PDS* knockout lines generated in this study (B). Blue-shaded sequences correspond to the gRNA target sites, located at nucleotides 132 to 151 for RNP1 and 147 to 166 for RNP2 within the PDS coding sequence (CDS). Insertions (ins) and deletions (del) are shown with indication of the number of nucleotides inserted (+) or deleted (–); "≥" denotes an insertion of unknown length.

The insertion consists of a 100-nucleotide fragment of plasmid pARG7 230, preceded by 4 nucleotides (nt) of unknown origin and the deletion of 5 nt. In mutant ΔA2, a deletion of the 4th and 5th nucleotides upstream of the PAM region, followed by the insertion of 560 nucleotides, resulted in a premature stop codon at position 70 of the *PDS* gene. Finally, the ΔD2 mutant incorporated a 54-nucleotide sequence of unknown origin, followed by a large plasmid-derived fragment of undetermined length, located nine nucleotides upstream of the PAM site. This insertion induced a premature stop codon resulting in functional disruption of the *PDS* gene. None of the analysed mutants had incorporated dsDR donor DNA sequences during the transformation event.

Another *PDS*-defective *Chlamydomonas* mutant, previously obtained by traditional mutagenesis by Tran et al. (2012), and named pds 1–2, has two punctual mutations resulting in the replacement of two amino acids (l64P and E143K). The E143K mutation took place in the conserved FAD-dependent oxidoreductase domain. These authors also obtained an insertional mutant, with an interruption in the fourth intron of the *PDS gene*, that resulted in the lack of carotenoids and the accumulation of phytoene.

3.3 | Phenotypical Characterization of PDS-Knockout *Chlamydomonas* Mutants

All *PDS* knockout mutant lines isolated were highly sensitive to light and exhibited reduced growth rates. Moreover, these transformant lines were found to be quite unstable, becoming non-viable or recovering to the original green phenotype after several divisions, suggesting that the loss of *PDS* function imposes a strong selective pressure favoring the emergence of revertant (Figure 4). This confirms the crucial role of carotenoid pigments in many fundamental molecular processes and highlights the central importance of the PDS enzyme in the pathway. To accurately characterize the phenotype and establish a direct correlation between the observed traits and *PDS* gene disruption, the analysis was conducted using three of the obtained *PDS*-Knockout mutant lines.

The white phenotype of the selected lines, ΔE10, ΔA2, and ΔD2 could be readily observed when grown on agar plates and in liquid cultures (Figure 5A–E). To obtain cultures of higher cellular density, the selected lines were grown in liquid medium in the dark for 3–4 weeks. After this growth period, cells were harvested by centrifugation and, when necessary, subjected to an additional purification step using fluorescence-assisted cell sorting (FACS) to separate white *PDS* knockout mutants from non-knockout co-transformants or reverted transformants based on chlorophyll fluorescence, as described in Materials and Methods (Figure S1). The pigment profile of the selected *PDS* knockout transformants was studied by HPLC-DAD (Figure 5F) and their morphology observed by optical and transmission electron microscopy (Figure 6).

The chromatographic separation of pigments revealed that the parental strain of *Chlamydomonas* had a typical pigment profile with β-carotene, lutein, and violaxanthin as major carotenoids (Table S3), in addition to chlorophylls *a* and *b*. Phytoene, which exhibits a maximum absorbance at 288 nm,

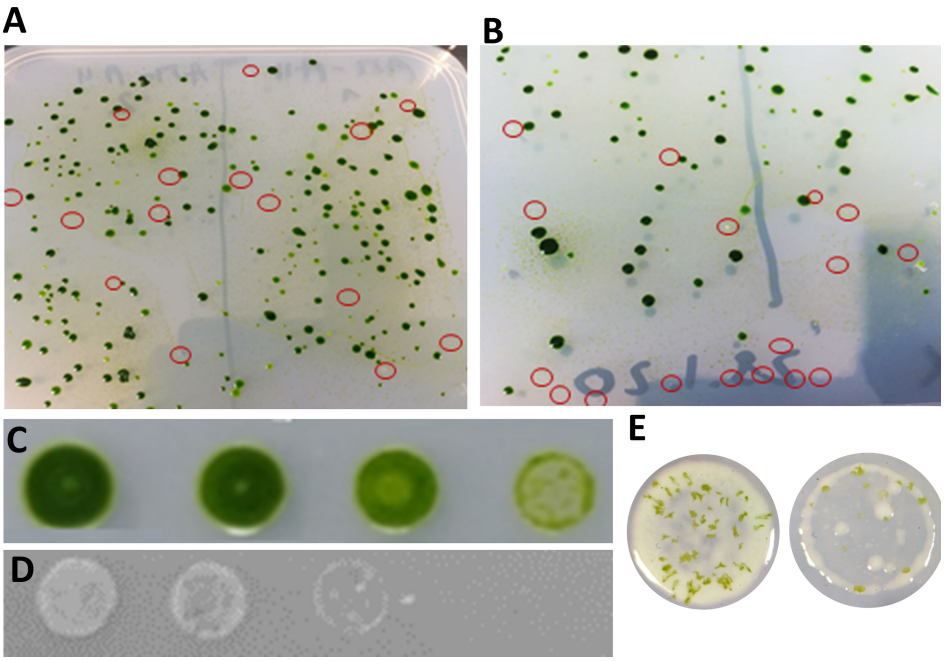

FIGURE 4 | Co-transformation and growth of a representative transformant line. (A-B) View of colonies obtained following co-transformation with the selectable plasmid pARG7-230 and ribonucleoprotein complexes RNP1 (A) and RNP2 (B). White colonies are indicated by red circles. (C, D) Spot plate assay comparing growth of the parental strain (C) and a representative, ΔA2 *PDS*-KO transformant (D). Two-fold serial dilutions of cultures with the same initial cell density (2×10^6 cells mL^{-1}) were spotted and incubated in the dark for 3 weeks. (E) A detailed view of spot plates of the *PDS*-KO transformants after 4 weeks of dark incubation shows the emergence of incipient revertants.

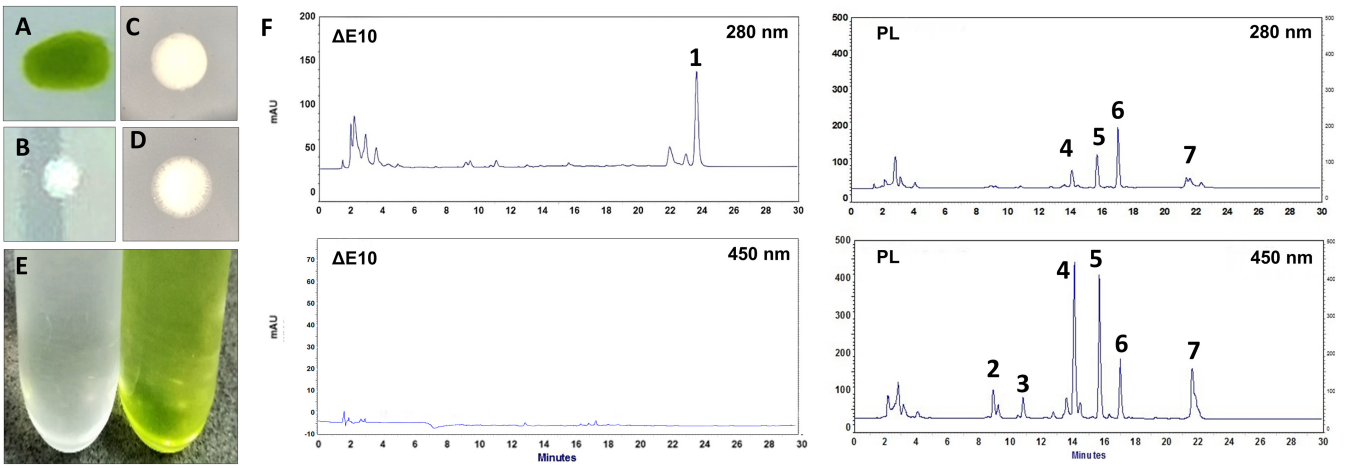

FIGURE 5 | Phenotypic characterization of selected *PDS* knockout lines. Parental (A) and *PDS*-knockout ΔA2 (B), ΔE10 (C), ΔD2 (D) colonies. (E) Comparison of parental and *PDS*-knockout lines grown in liquid cultures under dark conditions. (F) High-performance liquid chromatography (HPLC) profiles of the parental line (PL) and a representative knockout mutant (ΔE10) recorded at two wavelengths. Peaks: 1, phytoene; 2, neoxanthin–loroxanthin; 3, violaxanthin; 4, lutein; 5, chlorophyll b; 6, chlorophyll a; 7, β-carotene.

was not detectable in the parental line, as it is rapidly converted into downstream colored carotenoids. The transformant lines, on the contrary, contained the uncolored phytoene as the unique carotenoid and had no traces of colored carotenoids or chlorophylls (Figure 5F). Interestingly, although carotenoid-deficient *Chlamydomonas* mutants are unable to synthesize chlorophyll and therefore appear white, mutants in which chlorophyll biosynthesis is blocked can still produce carotenoids and appear as orange or yellow cells, as demonstrated in *Chlamydomonas* (Meinecke et al. 2010) and other chlorophytes (Xie et al. 2025).

The generation of *PDS* knockout transformants in *Chlamydomonas* has been particularly challenging. In fact, all carotenoid-deficient mutants reported in previous studies were either affected in *PSY* (McCarthy et al. 2004) or only partially affected in *PDS*, until the generation of the complete *PDS* knockout mutant pds1-2 by Tran and co-workers (Tran et al. 2012). The extreme light sensitivity, poor plating efficiency, and low growth rate have made it difficult to study the physiological and metabolic effect of colored carotenoid deficiency and phytoene accumulation in microalgae. The observation that *PDS* mutants are more difficult to grow than *PSY* mutants, which also have

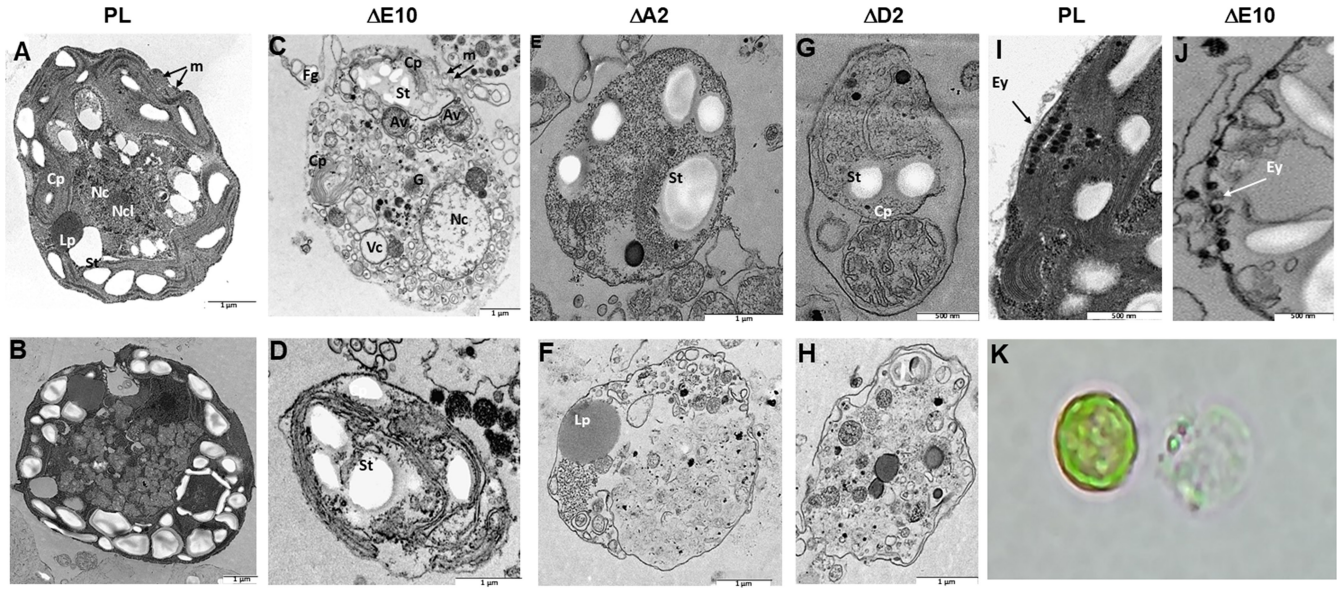

FIGURE 6 | Ultrastructure of parental and *PDS*-knockout lines of *Chlamydomonas reinhardtii*. (A–H) Transmission electron microscopy (TEM) images showing the ultrastructure of parental line, PL (A, B), and *PDS*-knockout mutants ΔE10 (C, D), ΔA2 (E, F) and ΔD2 (G, H). (I, J) Detailed view of the eyespot and the ordered array of plastoglobuli, resembling an eyespot in parental and ΔE10 lines, respectively. (K) Optical microscopy images of representative parental (left) and *PDS*-KO mutant cells, corresponding to ΔE10 (right). Organelles identified in TEM images: Cp, chloroplast; Ey, eyespot; Fg, flagella; Lp, lipid droplet; m, mitochondria; Nc, nucleus; Ncl, nucleolus; Pg, plastoglobuli; Py, pyrenoid; St, starch granule; Vc, vacuole.

a complete lack of colored carotenoids but do not accumulate phytoene, led the authors to suggest that phytoene accumulation could be toxic to the algal cells (McCarthy et al. 2004). In *Arabidopsis*, Qin et al. (2007) described an albino mutant affected in the *PDS* enzyme, which, besides accumulating phytoene, exhibited a dwarf phenotype probably due to the deficiency of ABA, which has β-carotene as a metabolic precursor, and gibberellins, biosynthetically derived from a common terpenoid precursor (Qin et al. 2007). This led the authors to suggest that the accumulated phytoene could be involved in negative regulatory feedbacks.

3.4 | Ultrastructure of Parental and *PDS*-Knockout Lines of *Chlamydomonas reinhardtii*

When observed under light microscopy, the colorless transformant cells displayed a shape and size comparable to those of wild-type cells (Figure 6K). However, transmission electron microscopy (TEM) revealed severe alterations in the ultrastructural organization of the *PDS*-knockout mutants, with poorly developed chloroplasts and other structures, such as the eyespot, either absent or markedly altered (Figures 6 and S2–S4). Wild-type cells exhibited a typical cellular organization, characterized by a well-organized chloroplast with clearly defined, normal stacking thylakoid membranes (Figure 6A,B). In contrast, the absence of carotenoids and consequently of chlorophylls resulted in a complete disorganization of the chloroplast in the mutant strains (ΔE10, ΔA2, and ΔD2; Figure 6C–J). These mutants displayed varying degrees of ultrastructural defects in chloroplast morphology, including severe alterations in the thylakoid membrane, which appeared disrupted or severely disorganized with multiple invaginations of the chloroplast envelope and sparse, non-stacked membranes.

The eyespot, a peripherally located structure composed of two highly ordered layers of carotenoid-rich protein globules assembled over thylakoid membranes, could be clearly observed in the parental line (Figures 6 and S2) but not in the mutants. The eyespot enables *Chlamydomonas* to perceive light direction and intensity, thereby guiding phototaxis movement; Its size and composition are regulated by light, typically increasing under dark conditions (Trippens et al. 2012). A peripherally-localized structure containing consecutives plasglobules resembling those of the eyespot was observed in the *PDS*-KO mutant ΔE10 (Figure 6J). The absence of colored carotenoid and structured thylakoid membranes, which would normally support eyespot globules may be the underlying cause. It has been reported that zeaxanthin is essential for functional eyespot formation in *Euglena*, whereas in *C. reinhardtii*, the eyespot is predominantly composed of β-carotene-rich globules. (Tamaki, Ozasa, et al. 2023; Tamaki, Shinomura, and Mochida 2023). The white *Chlamydomonas* mutant *lts1-204*, which lacks phytoene and its derivative carotenoids, has been described to possess a disorganized mislocalized vestigial eyespot (Inwood et al. 2008).

The pyrenoid was not detected in either the mutants or the parental line cultured in the dark (Figure 6). It was only visible, albeit smaller and surrounded by a diminished starch sheath, when the parental line is grown under light conditions (Figure S3). It has been reported that in *Chlamydomonas* cells grown under mixotrophic conditions and exposed to moderate or high light intensities, the pyrenoid remains visible, although smaller and less pronounced (Polukhina et al. 2016; He et al. 2023), which is consistent with our observations.

Starch globules and vacuoles containing membrane structures are abundant in the *PDS*-KO mutants. Similar membrane-containing vacuoles have been observed in carotenoids-depleted lines obtained by either the mutation of phytoene

synthase or the inhibition of phytoene desaturase by the herbicide norflurazon, conditions that resulted in a strong induction of autophagy (Pérez-Pérez et al. 2012). The increase of vacuoles in the *PDS*-KO mutant cells can be a consequence of the recycling of the components of thylakoid membranes (Inwood et al. 2008).

Disorganized chloroplasts have also been reported in *C. reinhardtii* mutants deficient in phytoene synthase, such as lts1, characterized by a chloroplast envelope folding back on itself, but lacking any stacked thylakoid membrane (Inwood et al. 2008). Similarly, immature plastids were observed in a *PDS* mutant line of *Arabidopsis thaliana* (Qin et al. 2007). In this case, no thylakoid membrane system was detected and plastid development was arrested at a proplastid stage.

These observations are consistent with the well-established essential role of carotenoids in photosystems assembly (Santabarbara et al. 2015) and with numerous studies in higher plants and microalgae that have demonstrated that, in the absence of carotenoids, reactive molecules such as singlet oxygen and triplet chlorophyll are inefficiently quenched, resulting in the oxidative degradation of chlorophylls and photosynthetic proteins, thereby compromising the structural and functional integrity of the photosystems (Frank and Brudvig 2004).

The *PSY*-deficient *Chlamydomonas* Its1 mutant exhibited, as do *PDS*-KO mutants, absence of a pyrenoid, disorganization of the eyespot, autophagic vacuoles, and accumulation of starch. Siu et al. (1976) found similarities between the ultrastructure of white *Chlamydomonas* and natural albine algae of the Polytoma group, which have a pigment-less plastid (leucoplast) without stacked thylakoids. No ultrastructural microscopy analysis of any *PDS* mutants of *Chlamydomonas* has been described to date.

These observations corroborate that carotenoids are essential structural components of the photosystems, where they not only contribute significantly to the stabilization of pigment–protein complexes but also play a crucial role in protecting against photooxidative stress, as previously reported (Zakar et al. 2016). The importance of this protective function is well established, as transformants in which carotenoid biosynthesis is completely impaired—either through gene mutation or the application of chemical inhibitors—exhibit extreme light sensitivity and markedly reduced growth (León et al. 2005; Vila et al. 2008; Molina-Márquez et al. 2019).

3.5 | Differential Gene Expression Profile Between Parental and *PDS*-KO Mutant Strains

To investigate differences in gene expression between the parental strain and the carotenoid-deficient microalgal mutants, a transcriptomic analysis was performed, and the profiles of differentially expressed (DE) genes were systematically characterized.

Total RNA was obtained from 6 biological replicates of the parental line and from six samples representing three different mutant lines (ΔD2, ΔA2, and ΔE10), all cultured in the dark with acetate as carbon source. All RNA samples with RIN values between 7.0 and 9.7 were reverse-transcribed into cDNA, amplified, and sequenced as detailed in materials and methods section. An average number of 8,105,069 reads per sample was obtained, of which 92% passed quality filters. Following alignment to the *C. reinhardtii* reference transcriptome (v5.6) and removal of reads that mapped to multiple loci, between 11,700 and 14,900 predicted genes were identified in the parental line, whereas 3900–8530 predicted genes were identified in the *PDS* knockout transformant lines.

Differential expression analysis, comparing parental strain and *PDS* knockout transformants, revealed 1703 genes exhibiting significant expression changes, defined by a $\log_2$ fold change ≥ 1 or ≤ -1 and a false discovery rate (FDR) < 0.05 5. A complete list of the DE genes is shown in Supporting Information (Table S4). Among these, 213 genes were up-regulated and 1490 were down-regulated. Principal component analysis (PCA) revealed that, despite considerable intra-group variability among replicates, a clear distinction between the parental and mutant lines was evident (Figure S5). The expression profiles of selected genes involved in the carotene biosynthesis pathway were further validated by quantitative real-time PCR (qRT-PCR) (Figure S6).

Functional enrichment analysis of differentially expressed genes between the parental strain and *PDS* knockout transformants revealed distinct gene expression patterns across various metabolic pathways involved in key biological processes and in the development of essential cellular components (Figure 7). For example, significant differential expression was observed in genes associated with anabolic processes, including the biosynthesis of organic acids, carbohydrate derivatives, and proteins. Genes involved in cellular transport and localization of macromolecules, peptides, and proteins also exhibited altered expression. Numerous genes related to vesicle formation and membrane trafficking were among those differentially expressed, reflecting alterations in protein secretion and endomembrane recycling processes, which are particularly active under stress conditions. This is consistent with the increased number of vacuoles and the modifications observed in the membranous system of the mutants (Figure 6). Interestingly, the depletion of carotenoid biosynthesis has been described as one of the factors that can trigger autophagy in *Chlamydomonas reinhardtii* (Pérez-Pérez et al. 2012). It has also been reported that *Chlamydomonas* mutants defective in *PSY*, or treated with bleaching herbicides that block *PDS*, exhibit constitutive autophagy, which is characterized by abnormal membrane structures and numerous large vacuoles (Couso et al. 2018; Chouhan et al. 2022).

Additionally, genes linked to photosynthesis and implicated in the biogenesis of thylakoid membranes and photosystem components were prominently represented in the functional analysis, with the majority showing downregulation. Carotenoids are not only light-harvesting and photoprotective pigments, but they also play a structural role in photosystem (PS) assembly and stability. Classical studies have demonstrated that the inhibition of carotenoid biosynthesis, either through chemical blockage of the pathway or through mutations in genes encoding their enzymes, profoundly affects photosystem assembly and viability of algal (Depka et al. 1998; McCarthy et al. 2004; Santabarbara et al. 2013), cyanobacteria (Tóth et al. 2015), and plants (Qin et al. 2007). The resolution of the *Chlamydomonas*

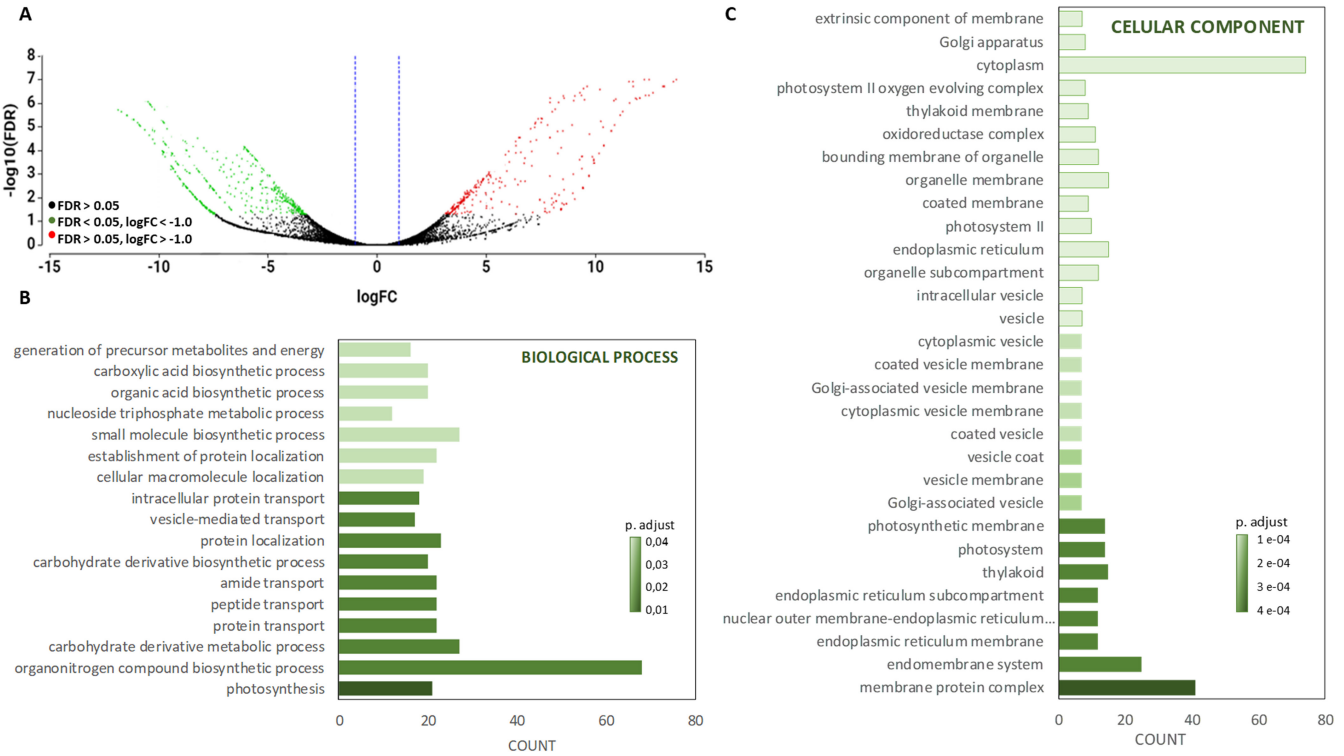

FIGURE 7 | Differential expression and functional analysis of the parental strain and *PDS* knockout mutants of *C. reinhardtii*. Total RNA was extracted from six biological replicates of the parental line (WT) and from six samples representing three independent mutant lines (ΔD2, ΔA2, and ΔE10), all cultured in the dark with acetate as the carbon source. (A) Volcano plot of statistical significance, false discovery rate (FDR) versus fold change (FC). (B) Classification of differentially expressed genes (DEGs) according to biological processes. (C) Classification of DEGs according to cellular components. Red and green dots indicate significantly differentially expressed genes (FDR ≤ 0.05; and $\log_2$FC > 1 or < −1, respectively), whereas black dots represent genes without significant fold change. Bars length corresponds to the number of genes annotated with the given GO term. The bar color captures the level of significance from less significant (light green) to more significant (dark green).

PSI–LHCI (8H2U) and PSII–LHCII (6KAC, 6KAD) complexes, as well as the PSI–LHCI–LHCII (7D0J) supercomplex, and other assembly intermediates, by X-ray diffraction or cryo-electron microscopy revealed the organization and assembly of the core photosystem and light-harvesting complex subunits (LHCI and LHCII), as well as the arrangement of their associated pigments (Shen et al. 2019; Huang et al. 2021). In *Chlamydomonas*, *β*-carotene is present in both the core and antenna complexes of the photosystems. It has traditionally been regarded as an essential component of the photosystem core complexes, whereas xanthophylls are associated with the light-harvesting antennae of both photosystems (Pineau et al. 2001). The xanthophylls lutein and zeaxanthin have been shown to be interchangeable in *Chlamydomonas* mutants lacking lutein (Polle et al. 2001). Moreover, a recent study in *Arabidopsis* demonstrated that astaxanthin can substitute for *β*-carotene in photosystems, suggesting a broader role for xanthophylls in the stabilization of photosynthetic complexes than previously recognized (Xu et al. 2020).

In the *PDS*-KO mutants generated in this study, neither colored carotenoids nor xanthophylls are synthesized, and the linear, colorless carotenoid phytoene cannot fulfill the protective and structural roles of its derivatives. In the absence of colored carotenoids, cells actively downregulate the main pathways for the synthesis of the photosystem components, chlorophyll and carotenoids (Table S4, Figure S7), which is consistent with previous studies that report repression of chlorophyll biosynthesis and degradation of chlorophylls and chlorophyll-binding proteins under stress in *C. reinhardtii* (Santabarbara et al. 2013; Zakar et al. 2016).

A more detailed analysis of the DE genes classified by metabolic pathways of interest is shown in Table 1. Photosynthesis-related genes, including those involved in the biosynthesis of chlorophylls and components of photosystems and light-harvesting complexes are downregulated. One interesting exception is PSBS3, which showed a $\log_2$ fold change greater than 10. This protein is a component of photosystem II and has been defined in *C. reinhardtii* as a putative effector of NPQ (see *Chlamydomonas* Library Project: https://www.chlamylibrary.org/index). However, it shares limited sequence identity with *PsbS1* and *PsbS2* and has been far less studied than these two paralogues, which encode nearly identical proteins and are functionally very similar. *PsbS1* and *PsbS2* appear to act primarily as transient modulators or activators of photoprotection by sensing lumen acidification and initiating NPQ-dependent photoprotective pathways, whose major molecular effector is LHCSR3, encoded by the *LHCSR3.1* and *LHCSR3.2* genes (Correa-Galvis et al. 2016; Redekop et al. 2020; Arend et al. 2023; Ruiz-Sola et al. 2023). In our study, the expression of *PsbS1* (Cre01.g016600), PsbS2 (Cre01.g016750), and *LHCSR3* (Cre08.g367500) showed a substantial, although not statistically significant, reduction in the *PDS*-KO mutants, with both FDR and *p*-values above 0.05,

TABLE 1 | Genes associated with key metabolic pathways exhibiting significant transcriptional changes in the **PDS**-KO mutant relative to the parental strain.

Name abbreviation	ID (JGI v5.6)	Log_2 FC	FDR value	Description
Photosynthesis/Chloroplast component				
PsaE	Cre10.g420350	−2.8	4.93E-02	Subunit IV of PSI
PsaG	Cre12.g560950	−2.9	2.29E-02	Subunit V of PSI
PsaL	Cre12.g486300	−3.1	2.45E-02	Subunit L of PSI
PSAN1	Cre02.g082500	−2.8	7.92E-03	Subunit N of PSI
PsbO	Cre09.g396213	−2.6	4.07E-02	Oxygen evolution enhancer protein 1 of PSII
Psb27	Cre05.g243800	−3.2	5.51E-03	Protein involve in PSII biogenesis
CGLD14	Cre10.g446350	−4.5	2.39E-03	PSBP Domain-containing protein 3 chloroplastic of PSII
PSBP3	Cre12.g509050	−4.1	4.23E-03	PsbP-like protein of thylakoid lumen of PSII
PSBR1	Cre06.g261000	−2.6	8.17E-03	Subunit R of PSII
PSBY1	Cre10.g452100	−2.6	9.53E-03	Ycf32-related polyprotein of PSII
PSBP1	Cre12.g550850	−2.6	2.37E-02	Oxygen evolution enhancer protein 2 of PSII
PSBQ1	Cre08.g372450	−2.5	3.10E-02	Oxygen evolution enhancer protein 3 of PSII
PSBO1	Cre09.g396213	−2.6	4.07E-02	Oxygen evolution enhancer protein 1 of PSII
PSBP	Cre16.g678851	−9.3	3.54E-02	PsbP-like protein of thylakoid lumen of PSII
PSBX1	Cre02.g082750	−2.8	4.07E-02	Reaction center subunit X of PSII
PSBS3	Cre03.g146147	12.2	6.70E-03	Involved in photoprotection of PSII
LHCA8	Cre06.g272650	−3.4	3.55E-02	Light-harvesting chlorophyll-a/b protein 8 of PSI
LHCB5	Cre16.g673650	−3.2	1.34E-02	Light-harvesting chlorophyll-a/b protein 5 of PSII
ATPC1	Cre06.g259900	−2.4	3.22E-02	Chloroplast ATP syntethase gamma chain
	Cre05.g241450	−9.2	4.22E-02	Conserved Hypothetical Protein. Similar to the Chloroplast SRP Receptor. Involved in protein import into the Thylakoid.
	Cre02.g099350	−4.2	3.21E-02	Scavenger receptor cysteine-rich protein
	Cre12.g522950	−4.3	1.85E-02	Putative chloroplast septum site-determining protein MinD. Chloroplast-encoded in other Chlorophyte algae.
Pigments biosynthesis				
TSE2	Cre07.g313700	−2.7	3.37E-02	Glutamyl/glutaminyl-tRNA synthetase
CHLI1	Cre06.g306300	−2.4	3.76E-02	Magnesium chelatase CHLI1 subunit
CTH1	Cre12.g510050	−2.8	7.25E-03	MPE oxidative cyclase CTH1 subunit
CHLG	Cre06.g294750	−4.1	7.50E-03	Chlorophyll synthase
POR1	Cre01.g015350	−2.6	3.47E-02	Light-dependent NADPH protochlorophyllide oxidoreductase
CLH1	Cre03.g148750	−3.0	9.27E-03	Chlorophyllase
CLD1	Cre16.g664350	−3.2	3.45E-02	Chlorophyll dephytylase
CAO1	Cre01.g043350	−2.5	4.07E-02	Chlorophyllide a oxigenase
D27A/CGLA	Cre16.g661150	−2.5	3.82E-03	β-Carotene isomerase

(Continues)

TABLE 1 | (Continued)

Name abbreviation	ID (JGI v5.6)	Log_2 FC	FDR value	Description
Carbon/Nitrogen assimilation				
RBCS1	Cre02.g120100	−3.8	5.98E-03	Ribulose-1,5-bi-phosphate carboxylase SS1
RBCS2	Cre02.g120150	−2.5	1.21E-02	Ribulose-1,5-bi-phosphate carboxylase SS2
PGK1	Cre11.g467770	−2.5	1.28E-02	Phosphoglycerate kinase
GAP3	Cre01.g010900	−2.5	2.46E-02	Glyceraldehyde-3-P dehydrogenase subunit A
CP12	Cre08.g380250	−2.8	3.90E-03	Calvin cycle protein CP12
GLN1	Cre02.g113200	−2.3	2.35E-02	Glutamine synthetase
NIT3	Cre06.g303050	−3.3	4.22E-02	Nitrate reductase NADH-cyt b5 reductase
Protein synthesis				
RPL30	Cre10.g420750	−2.2	3.13E-04	Large subunit ribosomal protein L30e
RPL10A	Cre02.g101350	−1.9	1.89E-03	Large ribosomal subunit protein L10a
RPS20	Cre16.g660150	−2.2	2.59E-02	Small subunit ribosomal protein S20e
MRPL32	Cre12.g558750	−9.8	3.03E-02	Mitochondrial ribosomal protein L32
PRPS16	Cre12.g494450	−2.4	1.57E-02	Chloroplast ribosomal protein S16
RPL35A	Cre10.g459250	−2.0	1.72E-02	Cytosolic 8S ribosomal protein L35a
RPS28	Cre12.g510450	−2.1	1.76E-02	Cytosolic 8S ribosomal protein LS28
RAF2	Cre01.g049000	−3.0	2.32E-02	RuBisCO assembly chaperone
Gene regulation				
	Cre08.g373350	9.3	4.23E-03	RNA-directed DNA polymerase
	Cre03.g174476	8.0	1.05E-02	C-type cyclin, CDK8 kinase-activating protein
	Cre27.g757397	11.6	3.73E-02	RNA-dependent DNA polymerase
	Cre28.g757597	11.7	9.22E-04	RNA-dependent DNA polymerase
	Cre06.g278276	11.8	5.98E-03	RNA-dependent DNA polymerase
	Cre09.g400145	8.6	4.89E-02	RNA-dependent DNA polymerase
	Cre06.g276150	10.9	3.88E-02	Sphingomyelin phosphodiesterase 2
	Cre06.g256800	10.8	3.88E-02	[Histone H3]-lysine(4) N-trimethyltransferase
	Cre06.g306726	10.5	2.52E-02	Precursor of chemotactic amidated peptide (Secretory)
	Cre03.g174476	8.0	1.05E-02	C-type cyclin, CDK8 kinase-activating protein
	Cre09.g400256	11.2	3.85E-02	Receptor protein-tyrosine kinase
Other upregulated genes with unknown function				
	Cre16.g692452	9.3	4.23E-03	Uncharactarized protein
	Cre03.g204500	13.0	3.47E-02	Uncharactarized protein
	Cre06.g304913	12.5	3.54E-02	Uncharactarized protein
	Cre06.g284376	12.1	3.60E-02	Uncharactarized protein
	Cre15.g643000	11.5	3.77E-02	Uncharactarized protein
	Cre06.g266276	11.4	8.46E-03	Uncharactarized protein
	Cre09.g400256	11.2	3.85E-02	Uncharactarized protein

(Continues)

TABLE 1 | (Continued)

Name abbreviation	ID (JGI v5.6)	Log_2 FC	FDR value	Description
	Cre02.g143087	7.0	4.03E-02	Uncharacterized protein
	Cre09.g398660	7.0	4.07E-02	Uncharacterized protein
	Cre02.g141226	6.6	4.29E-02	Uncharacterized protein

Note: Gene annotations were retrieved from the Phytozome database (*Chlamydomonas reinhardtii*, versions 5.6 or 6.1) and the Chlamydomonas Library Project (CLiP) database. The values for the logarithm of the fold change (log2FC), the statistical significance (FDR), and the description of each gene are shown. Red and green shaded log_2 FC values represent repressed and induced genes, respectively.

whereas the expression pattern of PSBS3 in the *PDS*-KO mutants differed markedly from that of its paralogues.

The carotenoid biosynthetic pathway is also affected in the *PDS*-KO mutant, with several genes largely downregulated, as ζ-carotene desaturase (*ZDS*) and the isomerases (*Z-ISO, D27A, D27B*) strongly downregulated (Figure S5). The analysis of protein–protein interaction networks for PDS using the Search Tool for the Retrieval of Interacting Genes/Proteins, STRING v12.5 (Szklarczyk et al. 2025) confirms the existence of a close relation between PDS and other proteins involved in the carotenoid biosynthetic pathway, as well as with plastid terminal oxidases (Figure S8).

Under normal conditions, wild-type *Chlamydomona*s lines exhibit an upregulation of carotenoid biosynthetic pathway genes when exposed to stress conditions (Couso et al. 2012). The pronounced reduction of the thylakoid system observed in the transformants may lead to downregulation of the expression of genes coding for enzymes of the carotenoid biosynthesis (Figure S7), which are associated with the thylakoid membrane.

In addition, a strong downregulation of genes encoding enzymes involved in carbon assimilation pathways was observed, with particularly pronounced repression of the ribulose-1,5-bisphosphate carboxylase/oxygenase small subunits 1 and 2 (RBCS1 and RBCS2), consistent with the expected inability of PDS knockout mutants to assimilate CO_2. Disrupting the *PDS3* gene in *Arabidopsis* resulted in inhibition of genes involved in carotenoid and chlorophyll metabolic pathways, as well as several chlorophyll-binding proteins and Calvin cycle enzymes (Qin et al. 2007). This is consistent with our observations and supports the idea that the absence of carotenoids and chlorophyll in the white mutant leads to the repression of both light and dark reactions of photosynthesis and key components of the photosynthetic apparatus.

Glycolytic enzymes such as PGK1 and GAP3, as well as enzymes involved in nitrogen assimilation, including GLN1 and NIT3, are also significantly downregulated in the mutants. Although in general, conditions that inhibit photosynthesis tend to induce the glycolytic pathway in microalgae and plants (Yu et al. 2024), the changes observed in the *PDS*-KO mutants appear to result from the need to decelerate metabolism under stress conditions and to activate emergency responses that prioritize metabolic conservation and the maintenance of redox balance over ATP synthesis. Moreover, some plant GAPDH isoforms, beyond their canonical role in glycolysis, have been shown to participate in the regulation of reactive oxygen species (ROS) homeostasis, autophagy, and plant immune responses (Henry et al. 2015).

On the other hand, the pronounced downregulation of numerous genes encoding components of both the small and large ribosomal subunits suggests a global reduction in the protein synthesis capacity of the mutant. Suppression of ribosome biogenesis is a well-documented response to oxidative stress, nutrient deprivation, and other conditions that lead to growth arrest (Gonzalez and Ynalvez 2023).

Conversely, the genes most strongly upregulated in the PDS-knockout transformants encode regulatory or signaling enzymes, such as receptor protein-tyrosine kinases (RTKs), cyclin kinases, histone methylases, and several RNA-directed DNA polymerases. These reverse transcriptases are intrinsically associated with the activity of mobile genetic elements known as retrotransposons. The genome of *Chlamydomonas reinhardtii* contains several types of retrotransposons, including well-characterized examples such as TOC1 and REM1 (Pérez-Alegre et al. 2005). These elements can be activated under various stress conditions, potentially as part of a self-defense response to extreme environments or as a result of impaired epigenetic silencing mechanisms that normally repress retrotransposon activity.

Differential expression analysis of these *PDS*-KO transformants indicates that microalgae lacking colored carotenoids exhibit a drastic metabolism reduction. Moreover, several genes with no previously assigned function but exhibiting high fold-change values were found to be overexpressed in the transformants. These genes are likely involved in the response to extreme stress conditions.

4 | Conclusions

The efforts previously done to obtain phytoene desaturase knockout mutants in microalgae yielded partial or total PDS-deficient mutants by random traditional or insertional mutagenesis. In this work, several targeted *PDS* knockout mutant lines have been produced by a reverse genetics approach using CRISPR-Cas9 RNP complexes. sgRNAs specifically guided the RNP complexes to the first exon of the *PDS* gene and cleaved it, inactivating the biosynthesis of colored carotenoids in *C. reinhardtii*. This confirms that the delivery of preassembled RNP complexes is an adequate method for gene silencing; it overcomes the difficulties found for the efficient expression of Cas9 in *Chlamydomonas*. In all the generated transformants, the cleaved DNA was repaired by non-homologous end-joining (NHEJ). All the obtained knockout transformants exhibited a white phenotype, characterized by the complete absence of colored carotenoids and chlorophylls, resulting in the accumulation of phytoene. In addition, all mutants displayed disorganized chloroplasts with a reduced thylakoid content and exhibited

extreme light sensitivity. Consistent with these observations, enzymes associated with carbon assimilation, chlorophyll and carotenoid biosynthesis, photosystem assembly, and ribosome biogenesis were significantly downregulated in *PDS*-KO transformants, in agreement with the findings obtained from transmission electron microscopy (TEM).

In contrast, transcripts encoding proteins with regulatory functions, including cyclin-dependent kinases, histone methyltransferases, or RNA-dependent DNA polymerases, were significantly upregulated. Moreover, the transcriptomic data indicate that genes implicated in membrane remodeling, vesicle trafficking, and diverse cellular stress responses were also differentially expressed, highlighting the broad cellular impact of carotenoid depletion and the pivotal role of carotenoids in maintaining photosynthetic and cellular homeostasis.

Author Contributions

Ana M. Molina-Márquez, Rosa León: conceptualization and methodology, writing – original draft. Ana M. Molina-Márquez, Simon Kelterborn: investigation. Ana M. Molina-Márquez, Miguel Pérez-Rodríguez, Rosa León: formal analysis. Rosa León, Javier Vigara, Peter Hegemann: supervision and funding acquisition. Ana M. Molina-Márquez, Rosa León, Javier Vigara, Peter Hegemann, Simon Kelterborn, Miguel Pérez-Rodríguez: writing – review and editing. All authors read and approved the final manuscript.

Acknowledgments

We thank Mr. Molina Grande-Caballero for support in bioinformatics treatment, and Dr. Romero-Campero from the University of Seville for assistance in the use of *AlgaeFun with maracas* software. We also acknowledge the support of Dra. Alicia Orea and Dra. Maria Jose Castro-Pérez, from the Institute of Plant Biochemistry and Photosynthesis (IBVF) and Institute of Biomedicine (IBIS), respectively, in FACS determinations.

Funding

This work was supported by the Regional Development Fund through the Agencia Estatal de Investigación-MCIN/AEI/10.13039/501100011033-(research grants 2019-110438RB-C22 and PID2022-140995OB-C21) and the German Research Foundation (DFG) (Project: 426566805, PH). P.H is a Hertie Professor and funded by the Hertie Foundation. Funding for open access charge: Universidad de Huelva/CBUA is acknowledged.

Disclosure

Generative AI was not used in this manuscript.

Data Availability Statement

The data that support the findings of this study are available within the article and in the Supporting Information of this article. Differentially expressed genes (DEGs) identified through RNA-seq analysis are publicly available at Zenodo (DOI: 10.5281/zenodo.18211856). The raw sequencing data have been deposited in the NCBI Sequence Read Archive (SRA) database under BioProject accession PRJNA1417634.

References

Absolute Markets Insights. 2023. "Global Phytoene Market 2022 Outlook by Product Type, Distribution Channel and End-User | Trends and Forecast to 2030." Accessed January 8, 2026. https://www.openpr.com/news/2952640/global-phytoene-market-2022-outlook-by-product-type.

Arend, M., Y. Yuan, M. Á. Ruiz-Sola, N. Omranian, Z. Nikoloski, and D. Petroutsos. 2023. "Widening the Landscape of Transcriptional Regulation of Green Algal Photoprotection." *Nature Communications* 14: 2687. https://doi.org/10.1038/s41467-023-38183-4.

Baek, K., D. H. Kim, J. Jeong, et al. 2016. "DNA-Free Two-Gene Knockout in *Chlamydomonas reinhardtii* via CRISPR-Cas9 Ribonucleoproteins." *Scientific Reports* 6: 1–7. https://doi.org/10.1038/srep30620.

Britton, G., S. Liaaen-Jensen, and H. Pfander. 2004. *Carotenoids*. Birkhäuser Basel. https://doi.org/10.1007/978-3-0348-7836-4.

Carol, P., D. Stevenson, C. Bisanz, et al. 1999. "Mutations in the Arabidopsis Gene IMMUTANS Cause a Variegated Phenotype by Inactivating a Chloroplast Terminal Oxidase Associated With Phytoene Desaturation." *Plant Cell* 11: 57–68. https://doi.org/10.1105/tpc.11.1.57.

Chazan, A., I. Das, T. Fujiwara, et al. 2023. "Phototrophy by Antenna-Containing Rhodopsin Pumps in Aquatic Environments." *Nature* 615: 535–540. https://doi.org/10.1038/s41586-023-05774-6.

Chouhan, N., E. Devadasu, R. M. Yadav, and R. Subramanyam. 2022. "Autophagy Induced Accumulation of Lipids in pgrl1 and pgr5 of *Chlamydomonas reinhardtii* Under High Light." *Frontiers in Plant Science* 12: 752634. https://doi.org/10.3389/fpls.2021.752634.

Correa-Galvis, V., P. Redekop, K. Guan, et al. 2016. "Photosystem II Subunit PsbS Is Involved in the Induction of LHCSR Protein-Dependent Energy Dissipation in *Chlamydomonas reinhardtii*." *Journal of Biological Chemistry* 291, no. 33: 17478–17487. https://doi.org/10.1074/jbc.M116.737312.

Couso, I., M. E. Pérez-Pérez, E. Martínez-Force, et al. 2018. "Autophagic Flux Is Required for the Synthesis of Triacylglycerols and Ribosomal Protein Turnover in Chlamydomonas." *Journal of Experimental Botany* 69, no. 6: 1355–1367. https://doi.org/10.1093/jxb/erx372.

Couso, I., M. Vila, J. Vigara, et al. 2012. "Synthesis of Carotenoids and Regulation of the Carotenoid Biosynthesis Pathway in Response to High Light Stress in the Unicellular Microalga *Chlamydomonas reinhardtii*." *European Journal of Phycology* 47, no. 3: 223–232. https://doi.org/10.1080/09670262.2012.692816.

Depka, B., P. Jahns, and A. Trebst. 1998. "β-Carotene to Zeaxanthin Conversion in the Rapid Turnover of the D1 Protein of Photosystem II." *FEBS Letters* 424, no. 3: 267–270. https://doi.org/10.1016/S0014-5793(98)00188-4.

Felemban, A., J. Braguy, M. D. Zurbriggen, and S. Al-Babili. 2019. "Apocarotenoids Involved in Plant Development and Stress Response." *Frontiers in Plant Science* 10: 1–16. https://doi.org/10.3389/fpls.2019.01168.

Frank, H. A., and G. W. Brudvig. 2004. "Redox Functions of Carotenoids in Photosynthesis." *Biochemistry* 43, no. 27: 8607–8615. https://doi.org/10.1021/bi0492096.

Gemmecker, S., P. Schaub, J. Koschmieder, et al. 2015. "Phytoene Desaturase From *Oryza sativa*: Oligomeric Assembly, Membrane Association and Preliminary 3D-Analysis." *PLoS One* 10, no. 7: e0131717. https://doi.org/10.1371/journal.pone.0131717.

Gonzalez, D. I., and R. A. Ynalvez. 2023. "Comparison of the Effects of Nitrogen-, Sulfur- and Combined Nitrogen- and Sulfur-Deprivations on Cell Growth, Lipid Bodies and Gene Expressions in *Chlamydomonas reinhardtii* cc5373-sta6." *BMC Biotechnology* 23, no. 1: 35. https://doi.org/10.1186/s12896-023-00808-3.

Greiner, A., S. Kelterborn, H. Evers, G. Kreimer, I. Sizova, and P. Hegemann. 2017. "Targeting of Photoreceptor Genes in *Chlamydomonas reinhardtii* via Zinc-Finger Nucleases and CRISPR/Cas9." *Plant Cell* 29: 2498–2518. https://doi.org/10.1105/tpc.17.00659.

Grossman, A. R., M. Lohr, and C. S. Im. 2004. "*Chlamydomonas reinhardtii* in the Landscape of Pigments." *Annual Review of Genetics* 38, no. 1: 119–173. https://doi.org/10.1146/annurev.genet.38.072902.092328.

Gupta, P., and J. Hirschberg. 2022. "The Genetic Components of a Natural Color Palette: A Comprehensive List of Carotenoid Pathway Mutations in Plants." *Frontiers in Plant Science* 12: 1–19. https://doi.org/10.3389/fpls.2021.806184.

Haeussler, M., K. Schönig, H. Eckert, et al. 2016. "Evaluation of Off-Target and On-Target Scoring Algorithms and Integration Into the Guide RNA Selection Tool CRISPOR." *Genome Biology* 17, no. 1: 148. https://doi.org/10.1186/s13059-016-1012-2.

Hashimshony, T., F. Wagner, N. Sher, and I. Yanai. 2012. "CEL-Seq: Single-Cell RNA-Seq by Multiplexed Linear Amplification." *Cell Reports* 2, no. 3: 666–673. https://doi.org/10.1016/j.celrep.2012.08.003.

He, S., V. L. Crans, and M. C. Jonikas. 2023. "The Pyrenoid: The Eukaryotic CO_2-Concentrating Organelle." *Plant Cell* 35, no. 9: 3236–3259. https://doi.org/10.1093/plcell/koad157.

Hegemann, P. 1997. "Vision in Microalgae." *Planta* 203: 265–274.

Henry, E., N. Fung, J. Liu, G. Drakakaki, and G. Coaker. 2015. "Beyond Glycolysis: GAPDHs Are Multi-Functional Enzymes Involved in Regulation of ROS, Autophagy, and Plant Immune Responses." *PLoS Genetics* 11, no. 4: e1005199. https://doi.org/10.1371/journal.pgen.1005199.

Huang, Z., L. Shen, W. Wang, et al. 2021. "Structure of Photosystem I-LHCI-LHCII From the Green Alga *Chlamydomonas reinhardtii* in State 2." *Nature Communications* 12, no. 1: 1100. https://doi.org/10.1038/s41467-021-21362-6.

Im, S. C., and A. R. Grossman. 2002. "Identification and Regulation of High Light-Induced Genes in *Chlamydomonas reinhardtii*." *Plant Journal* 30, no. 3: 301–313. https://doi.org/10.1046/j.1365-313X.2001.01287.x.

Inwood, W., C. Yoshihara, R. Zalpuri, K. S. Kim, and S. Kustu. 2008. "The Ultrastructure of a *Chlamydomonas reinhardtii* Mutant Strain Lacking Phytoene Synthase Resembles That of a Colorless Alga." *Molecular Plant* 1, no. 6: 925–937. https://doi.org/10.1093/mp/ssn046.

Kelterborn, S., F. Boehning, I. Sizova, O. Baidukova, H. Evers, and P. Hegemann. 2022. "Gene Editing in Green Alga *Chlamydomonas reinhardtii* via CRISPR-Cas9 Ribonucleoproteins." In *Methods in Molecular Biology*, vol. 2379, 45–65. Humana Press Inc.

Koschmieder, J., M. Fehling-Kaschek, P. Schaub, et al. 2017. "Plant-Type Phytoene Desaturase: Functional Evaluation of Structural Implications." *PLoS One* 12, no. 11: e0187628. https://doi.org/10.1371/journal.pone.0187628.

León, R., M. Vila, D. Hernánz, and C. Vílchez. 2005. "Production of Phytoene by Herbicide-Treated Microalgae *Dunaliella bardawil* in Two-Phase Systems." *Biotechnology and Bioengineering* 92: 695–701. https://doi.org/10.1002/bit.20660.

Li, H., and R. Durbin. 2010. "Fast and Accurate Long-Read Alignment With Burrows-Wheeler Transform." *Bioinformatics* 26, no. 5: 589–595. https://doi.org/10.1093/bioinformatics/btp698.

Lichtenthaler, H. K. 1987. "Chlorophylls and Carotenoids: Pigments of Photosynthetic Biomembranes." *Methods in Enzymology* 148: 350–382. https://doi.org/10.1016/0076-6879(87)48036-1.

Lohr, M. 2023. "Carotenoids in Chlamydomonas." In *The Chlamydomonas Sourcebook*, 733–761. Elsevier.

Lohr, M., C. S. Im, and A. R. Grossman. 2005. "Genome-Based Examination of Chlorophyll and Carotenoid Biosynthesis in *Chlamydomonas reinhardtii*." *Plant Physiology* 138, no. 1: 490–515. https://doi.org/10.1104/pp.104.056069.

Mapelli-Brahm, P., P. Gómez-Villegas, M. L. Gonda, et al. 2023. "Microalgae, Seaweeds and Aquatic Bacteria, Archaea, and Yeasts: Sources of Carotenoids With Potential Antioxidant and Anti-Inflammatory Health-Promoting Actions in the Sustainability Era." *Marine Drugs* 21, no. 6: 340. https://doi.org/10.3390/md21060340.

Mapelli-Brahm, P., and A. J. Meléndez-Martínez. 2021. "The Colourless Carotenoids Phytoene and Phytofluene: Sources, Consumption, Bioavailability and Health Effects." *Current Opinion in Food Science* 41: 201–209. https://doi.org/10.1016/j.cofs.2021.04.013.

McCarthy, S. S., M. C. Kobayashi, and K. K. Niyogi. 2004. "White Mutants of *Chlamydomonas reinhardtii* Are Defective in Phytoene Synthase." *Genetics* 168, no. 3: 1249–1257. https://doi.org/10.1534/genetics.104.030635.

Meinecke, L., A. Alawady, M. Schroda, et al. 2010. "Chlorophyll-Deficient Mutants of *Chlamydomonas reinhardtii* That Accumulate Magnesium Protoporphyrin IX." *Plant Molecular Biology* 72, no. 6: 643–658. https://doi.org/10.1007/s11103-010-9604-9.

Meléndez-Martínez, A. J., C. M. Stinco, and P. Mapelli-Brahm. 2019. "Skin Carotenoids in Public Health and Nutricosmetics: The Emerging Roles and Applications of the UV Radiation-Absorbing Colourless Carotenoids Phytoene and Phytofluene." *Nutrients* 11, no. 5: 1093. https://doi.org/10.3390/nu11051093.

Mikami, K., and N. Murata. 2003. "Membrane Fluidity and the Perception of Environmental Signals in Cyanobacteria and Plants." *Progress in Lipid Research* 42, no. 6: 527–543. https://doi.org/10.1016/S0163-7827(03)00036-5.

Molina-Márquez, A., M. Vila, J. Vigara, A. Borrero, and R. León. 2019. "The Bacterial Phytoene Desaturase-Encoding Gene (CRTI) is an Efficient Selectable Marker for the Genetic Transformation of Eukaryotic Microalgae." *Metabolites* 9, no. 3: 49. https://doi.org/10.3390/metabo9030049.

Morón-Ortiz, Á., A. A. Karamalegkos, P. Mapelli-Brahm, M. Ezcurra, and A. J. Meléndez-Martínez. 2024. "Phytoene and Phytoene-Rich Microalgae Extracts Extend Lifespan in *C. elegans* and Protect Against Amyloid-β Toxicity in an Alzheimer's Disease Model." *Antioxidants* 13, no. 8: 931. https://doi.org/10.3390/antiox13080931.

Norris, S. R., T. R. Barrette, and D. Dellapenna. 1995. "Genetic Dissection of Camtenoid Synthesis in Arabidopsis Defines Plastoquinone as an Essential Component of Phytoene Desat Urat Ion." *Plant Cell* 7: 2139.

Novoveská, L., M. E. Ross, M. S. Stanley, R. Pradelles, V. Wasiolek, and J. F. Sassi. 2019. "Microalgal Carotenoids: A Review of Production, Current Markets, Regulations, and Future Direction." *Marine Drugs* 17, no. 11: 640. https://doi.org/10.3390/md17110640.

Perazzoli, G., C. Luque, A. León-Vaz, et al. 2024. "Preliminary Assessment of the Protective and Antitumor Effects of Several Phytoene-Containing Bacterial and Microalgal Extracts in Colorectal Cancer." *Molecules* 29, no. 21. https://doi.org/10.3390/molecules29215003.

Pérez-Alegre, M., A. Dubus, and E. Fernández. 2005. "REM1, a New Type of Long Terminal Repeat Retrotransposon in *Chlamydomonas reinhardtii*." *Molecular and Cellular Biology* 25, no. 23: 10628–10638. https://doi.org/10.1128/mcb.25.23.10628-10638.2005.

Pérez-Pérez, M. E., I. Couso, and J. L. Crespo. 2012. "Carotenoid Deficiency Triggers Autophagy in the Model Green Alga *Chlamydomonas reinhardtii*." *Autophagy* 8, no. 3: 376–388. https://doi.org/10.4161/auto.18864.

Pfaffl, M. V. 2001. "A New Mathematical Model for Relative Quantification in Real-Time RT PCR." *Nucleic Acids Research* 29, no. 9: e45. https://doi.org/10.1093/nar/29.9.

Pineau, B., C. Gérard-Hirne, and C. Selve. 2001. "Carotenoid Binding to Photosystems I and II of *Chlamydomonas reinhardtii* Cells Grown Under Weak Light or Exposed to Intense Light."

Polle, J. E. W., K. K. Niyogi, and A. Melis. 2001. "Absence of Lutein, Violaxanthin and Neoxanthin Affects the Functional Chlo-Rophyll Antenna Size of Photosystem-II but Not That of Photosystem-I in the Green Alga *Chlamydomonas reinhardtii*." *Plant and Cell Physiology* 42, no. 5: 482–491. https://doi.org/10.1093/pcp/pce057.

Polukhina, I., R. Fristedt, E. Dinc, P. Cardol, and R. Croce. 2016. "Carbon Supply and Photoacclimation Cross Talk in the Green Alga *Chlamydomonas reinhardtii*." *Plant Physiology* 172, no. 3: 1494–1505. https://doi.org/10.1104/pp.16.01310.

Qin, G., H. Gu, L. Ma, et al. 2007. "Disruption of Phytoene Desaturase Gene Results in Albino and Dwarf Phenotypes in Arabidopsis by Impairing Chlorophyll, Carotenoid, and Gibberellin Biosynthesis." *Cell Research* 17, no. 5: 471–482. https://doi.org/10.1038/cr.2007.40.

Redekop, P., N. Rothhausen, N. Rothhausen, et al. 2020. "PsbS Contributes to Photoprotection in *Chlamydomonas reinhardtii* Independently of Energy Dissipation." *Biochimica et Biophysica Acta - Bioenergetics* 1861, no. 5–6: 148183. https://doi.org/10.1016/j.bbabio.2020.148183.

Robinson, M. D., D. J. McCarthy, and G. K. Smyth. 2009. "edgeR: A Bioconductor Package for Differential Expression Analysis of Digital Gene Expression Data." *Bioinformatics* 26, no. 1: 139–140. https://doi.org/10.1093/bioinformatics/btp616.

Rodriguez-Concepcion, M., J. Avalos, M. L. Bonet, et al. 2018. "A Global Perspective on Carotenoids: Metabolism, Biotechnology, and Benefits for Nutrition and Health." *Progress in Lipid Research* 70: 62–93. https://doi.org/10.1016/j.plipres.2018.04.004.

Romero-Losada, A. B., C. Arvanitidou, P. de los Reyes, M. García-González, and F. J. Romero-Campero. 2022. "ALGAEFUN With MARACAS, microALGAE FUNctional Enrichment Tool for MicroAlgae RnA-Seq and Chip-Seq AnalysiS." *BMC Bioinformatics* 23, no. 1: 113. https://doi.org/10.1186/s12859-022-04639-5.

Ruiz-Sola, M. Á., S. Flori, Y. Yuan, et al. 2023. "Light-Independent Regulation of Algal Photoprotection by CO_2 Availability." *Nature Communications* 14: 1977. https://doi.org/10.1038/s41467-023-37800-6.

Santabarbara, S., A. Agostini, A. P. Casazza, G. Zucchelli, and D. Carbonera. 2015. "Carotenoid Triplet States in Photosystem II: Coupling With Low-Energy States of the Core Complex." *Biochimica et Biophysica Acta - Bioenergetics* 1847, no. 2: 262–275. https://doi.org/10.1016/j.bbabio.2014.11.008.

Santabarbara, S., A. P. Casazza, K. Ali, et al. 2013. "The Requirement for Carotenoids in the Assembly and Function of the Photosynthetic Complexes in *Chlamydomonas reinhardtii*." *Plant Physiology* 161, no. 1: 535–546. https://doi.org/10.1104/pp.112.205260.

Schüler, L. M., P. S. C. Schulze, H. Pereira, L. Barreira, R. León, and J. Varela. 2017. "Trends and Strategies to Enhance Triacylglycerols and High-Value Compounds in Microalgae." In *Algal Research*, vol. 25, 263–273. Elsevier B.V.

Shen, L., Z. Huang, S. Chang, et al. 2019. "Structure of a C2S2M2N2-Type PSII–LHCII Supercomplex From the Green Alga *Chlamydomonas reinhardtii*." *Proceedings of the National Academy of Sciences of the United States of America* 116, no. 42: 21246–21255. https://doi.org/10.1073/pnas.1912462116.

Simmini, S., M. Bialecka, M. Huch, et al. 2014. "Transformation of Intestinal Stem Cells Into Gastric Stem Cells on Loss of Transcription Factor Cdx2." *Nature Communications* 5: 5728. https://doi.org/10.1038/ncomms6728.

Siu, C.-H., H. Swift, and K.-S. Chiang. 1976. "Characterization of Cytoplasmic and Nuclear Genomes in the Colorless Alga Polytoma I. Ultrastructural Analysis of Organelles." *Journal of Cell Biology* 69, no. 2: 352–370. https://doi.org/10.1083/jcb.69.2.352.

Sizova, I., S. Kelterborn, V. Verbenko, S. Kateriya, and P. Hegemann. 2021. "Chlamydomonas POLQ Is Necessary for CRISPR/Cas9-Mediated Gene Targeting." *G3 (Bethesda, Md.)* 11, no. 7: jkab114. https://doi.org/10.1093/g3journal/jkab114.

Szklarczyk, D., K. Nastou, M. Koutrouli, et al. 2025. "The STRING Database in 2025: Protein Networks With Directionality of Regulation." *Nucleic Acids Research* 53, no. D1: D730–D737. https://doi.org/10.1093/nar/gkae1113.

Tamaki, S., K. Ozasa, T. Nomura, et al. 2023. "Zeaxanthin Is Required for Eyespot Formation and Phototaxis in *Euglena gracilis*." *Plant Physiology* 191, no. 4: 2414–2426. https://doi.org/10.1093/plphys/kiad001.

Tamaki, S., T. Shinomura, and K. Mochida. 2023. "Illuminating the Diversity of Carotenoids in Microalgal Eyespots and Phototaxis." *Plant Signaling & Behavior* 18, no. 1: 2257348. https://doi.org/10.1080/15592324.2023.2257348.

Tóth, T. N., V. Chukhutsina, I. Domonkos, et al. 2015. "Carotenoids are Essential for the Assembly of Cyanobacterial Photosynthetic Complexes." *Biochimica et Biophysica Acta (BBA) – Bioenergetics* 1847, no. 10: 1153–1165.

Tran, P. T., M. N. Sharifi, S. Poddar, R. M. Dent, and K. K. Niyogi. 2012. "Intragenic Enhancers and Suppressors of Phytoene Desaturase Mutations in *Chlamydomonas reinhardtii*." *PLoS One* 7, no. 8: e42196. https://doi.org/10.1371/journal.pone.0042196.

Trippens, J., A. Greiner, J. Schellwat, et al. 2012. "Phototropin Influence on Eyespot Development and Regulation of Phototactic Behavior in *Chlamydomonas reinhardtii*." *Plant Cell* 24, no. 11: 4687–4702. https://doi.org/10.1105/tpc.112.103523.

Ueki, N., T. Ide, S. Mochiji, et al. 2016. "Eyespot-Dependent Determination of the Phototactic Sign in *Chlamydomonas reinhardtii*." *Proceedings of the National Academy of Sciences of the United States of America* 113, no. 19: 5299–5304. https://doi.org/10.1073/pnas.1525538113.

Varela, J. C., H. Pereira, M. Vila, and R. León. 2015. "Production of Carotenoids by Microalgae: Achievements and Challenges." *Photosynthesis Research* 125, no. 3: 423–436. https://doi.org/10.1007/s11120-015-0149-2.

Vila, M., I. Couso, and R. León. 2008. "Carotenoid Content in Mutants of the Chlorophyte *Chlamydomonas reinhardtii* With Low Expression Levels of Phytoene Desaturase." *Process Biochemistry* 43, no. 10: 1147–1152. https://doi.org/10.1016/j.procbio.2008.06.014.

Xie, Y., W. Lin, W. Zhang, et al. 2025. "Chlorophyll-Deficient Triggers Heterotrophic Lutein-Directed Biosynthesis in a Novel Mutant Strain of Chlorella Sorokiniana (Chlorophyta): Process Characterization and Underlying Mechanism." *Aquaculture* 598: 741998. https://doi.org/10.1016/j.aquaculture.2024.741998.

Xu, P., V. U. Chukhutsina, W. J. Nawrocki, et al. 2020. "Photosynthesis Without β-Carotene." *eLife* 9: 1–16. https://doi.org/10.7554/ELIFE.58984.

Young, A., S. Orset, and A. Tsavalos. 1997. "Methods for Carotenoid Analysis." In *Handbook of Photosynthesis*, edited by M. Pessarakli, 59–622. Marcel Dekker.

Yu, W., F. Gong, K. Cao, X. Zhou, and H. Xu. 2024. "Multi-Omics Analysis Reveals the Molecular Mechanisms of the Glycolysis and TCA Cycle Pathways in Rhododendron Chrysanthum Pall. Under UV-B Stress." *Agronomy* 14, no. 9: 1996. https://doi.org/10.3390/agronomy14091996.

Zakar, T., H. Laczko-Dobos, T. N. Toth, and Z. Gombos. 2016. "Carotenoids Assist in Cyanobacterial Photosystem II Assembly and Function." *Frontiers in Plant Science* 7: 295. https://doi.org/10.3389/fpls.2016.00295.

Supporting Information

Additional supporting information can be found online in the Supporting Information section. **Table S1:** Primers designed to detect the regions targeted by Cas9-RNP complexes in the *PDS* gene. **Table S2:** Primers designed for qPCR validation of the transcript level of several carotene biosynthetic genes. **Table S3:** Carotenoid content of parental (CC-3403) and *PDS*-KO (ΔE10) *C. reinhardtii* lines cultured in the dark

at standard conditions. Values are related to dry weight and expressed as mean ± SD. **Figure S1:** Fluorescent assisted cytometer sorting out (FACS) analysis. Flow cytometry density plots showing red fluorescence (PE-Cy5, 670 nm) versus blue fluorescence (FITC, 530 nm). White, chlorophyll-deficient mutant cells can be distinguished from photosynthetic, chlorophyll-containing cells by the autofluorescence of chlorophyll detected through a red (670/40 nm) bandpass filter following excitation with a blue laser. The square represents the gate used to discriminate between the different populations. **Figure S2:** Transmission electron micrographs of the parental strain (PL) and the *PDS*-KO transformant (ΔE10). Both cell lines were grown in the dark. The rectangles highlight the structure of the eyespot in the wild type and the array of plastoglobuli that resemble a disorganized eyespot in the transformant, and correspond to panels I and J of Figure 6. **Figure S3:** Transmission electron micrographs of the parental strain grown in the dark (PL, dark) and in light (PL, light) (100 μE $m^{-2}s^{-1}$). **Figure S4:** Transmission electron micrographs of *PDS*-KO mutants (ΔE10, AΔ2) all grown in the dark. **Figure S5:** Principal component analysis (PCA) comparing the parental (WT) and mutant lines (ΔD2, ΔA2, ΔE10). **Figure S6:** Transcription levels of several carotenoid biosynthetic genes. Samples of control wild type (WT) and transformant (ΔA2 and ΔD2) cell lines, cultured in the dark with acetate as carbon source, were processed for mRNA isolation and reverse-transcription and the expression of the indicated genes analyzed by quantitative RT-PCR. Measurements were normalized to the *CBLP* endogenous gene and presented as fold-change relative to transcript levels of the parental line. Error bars represent 95% confidence intervals from three replicates. *CHYB*, β-carotene hydroxylase; *LCYB*, lycopene β-cyclase; *ZDS*, ζ-carotene desaturase. **Figure S7:** Partial view of KEGG pathway Cre00906-carotenoid biosynthesis- with indication of Gene name, Gene ID and $\log_2$ fold change (PDS-KO mutans vs. Parental line) as determined by EdgeR package with an adjusted $p < 0.01$. **Figure S8:** Protein–Protein association network for PDS with STRING tool. Network nodes represent proteins produced by a single, gene locus. colored nodes represent first shell of interactors, filled nodes represent proteins for which a 3D structure is known or predicted. The edges in the network represent both experimentally determined and predicted interactions, which may arise from physical associations, genomic proximity, co-expression patterns, or co-mentions in PubMed abstracts, as indicated in right panel.